ELSEVIER

Contents lists available at ScienceDirect

Construction and Building Materials

journal homepage: www.elsevier.com/locate/conbuildmat





Effect of water-based nanoclay and ambient temperature on rheological properties of UHPC pastes

Jiang Du, Pengwei Guo, Weina Meng

Department of Civil, Environmental and Ocean Engineering, Stevens Institute of Technology, Hoboken, NJ, USA

ARTICLE INFO

Keywords:
UHPC pastes
Water-based nanoclay suspension
Ambient temperature
Dynamic yield stress
Plastic viscosity
Thixotropy

ABSTRACT

Rheological properties of ultra-high-performance concrete (UHPC) pastes significantly impact the flowability and segregation resistance of UHPC, thus are of great importance to investigate. This study investigated the coupled effect of the water-based nanoclay suspension and ambient temperatures on rheological properties of UHPC pastes. Firstly, the water-based nanoclay was proved to show good compatibility with used PCE-based HRWR. Besides, the nanoclay content varied from 0 to 0.20% and the evaluated ambient temperatures were 10 $^{\circ}\text{C},$ 25 $^{\circ}\text{C},$ and 35 °C. Results showed that the addition of nanoclay and elevation of ambient temperatures significantly increased plastic viscosity and dynamic yield stress of UHPC pastes. The thixotropy of UHPC pastes was also enhanced, which was quantified by a bi-linear model including initial fluctuations of static yield stress (τ_{flor}) and thixotropy index (IA). The enhancement of rheological properties are closely related to the evolution of internal microstructure, including physical and chemical effects. The physical effects refer to the flocculation between particles: (1) the addition of nanoclay accelerated the flocculation by the electrostatic attraction forces; (2) the elevation of ambient temperatures accelerated the flocculation by promoting Brownian motions of particles. The chemical effects refer to the increased hydration reaction: (1) the nanoclay addition increased aluminates contents, thus promoting the hydration of C₃A to generate ettringite; (2) the elevation of ambient temperatures increased the dissolution of C₃A then promoted the hydration. More importantly, ettringite is the main hydration product to affect the rheological properties of UHPC pastes. This study revealed the coupled effect of water-based nanoclay and ambient temperature on rheology of UHPC pastes and will advance the large-scale application of the water-based nanoclay suspension.

1. Introduction

Ultra-high-performance concrete (UHPC) is a new family of advanced cementitious composites featuring superior mechanical performance and excellent durability [1–3]. It has been widely used in highway bridge constructions and architectures, such as precast girders and piles [4–6], field-cast connections and joints [7–10], jackets for columns [11], bridge deck overlays [12–15], roof lattices and claddings [16,17], and freeform pillars [18]. UHPC mixtures behave in unique rheological properties (i.e., dynamic yield stress, plastic viscosity, and thixotropy) [19], due to the extremely low water-to-binder ratio (e.g., w/b = 0.15–0.25) and high binder content.

For UHPC, the desired rheological properties are different for different application scenarios. For instance, in the case of deep elements (e.g., walls and piers), low dynamic yield stress and high thixotropy are expected, aiming to achieve good filling capacity and lower

lateral pressure on formworks [20,21]. For shallow elements (e.g., beams), an optimum plastic viscosity is required to uniformly disperse the steel fibers, thus achieving the maximum tensile properties [14]. In the case of sloped casting (e.g., bridge deck overlay), the optimum dynamic yield stress and high thixotropy are expected to enable the ease of placement and good shape stability [14]. For the application of 3D printing, the initial dynamic (static) yield stress of UHPC is carefully designed with high thixotropy, so that the proper extrudability and buildability can be secured [22]. As mentioned above, the proper control of the rheological properties is considered the key to ensuring the high quality of various UHPC applications. Previous studies summarized that the rheological properties of UHPC were influenced by the pastes, aggregates, and reinforced fibers [23,24]. Khayat et al. [19] indicated that the gradation of fine aggregates plays a critical role on rheological properties of UHPC. Compared to the uniformed or gap sand gradation, the continuous sand gradation can exhibit the lowest viscosity due to the

E-mail address: wmeng3@stevens.edu (W. Meng).

 $^{^{\}ast}$ Corresponding author.

high packing density. Besides, the addition of reinforced fibers generally increases the yield stress and viscosity of UHPC [25]. However, the effects from pastes are more complicated. This study focuses on the coupled effect of water-based nanoclay suspension and ambient temperatures on the rheological properties of UHPC pastes.

The rheological properties of UHPC pastes are dependent on the w/b, chemical admixtures, binder compositions, and ambient temperatures [19,26–29]. In the first place, the rheological properties of all cementbased materials are sensitive to w/b. For instance, Wang et al. [30] investigated the effect of w/b on rheological properties of UHPC mortars with fixed HRWR content of 1.4% (by mass of binder). Results revealed that, as the w/b decreased from 0.24 to 0.20, the dynamic yield stress was increased by 1500% and the plastic viscosity was increased by 100%. A minor change of w/b led to a dramatic increase in the rheological properties of UHPC mortar. Besides, superplasticizers, also known as high-range water reducers (HRWR), are the most important chemical admixtures to ensure the sufficient flowability for UHPC pastes with extremely low w/b. In past decades, several different types of HRWR were developed, including lignosulfonates (LS) type, polymelamine sulfonate (PMS) type, sulfonated melamine formaldehyde condensate (SMF) type, and polycarboxylate (PCE) type HRWR [31]. Among them, PCE-based HRWR shows the best water reduction ability which can achieve up to 40% water reduction due to the steric repulsion effect and retarded cement hydration effect [1]. For example, Feng et al. [32] investigated the effect of different PCE-based HRWR on rheological properties of cement pastes with 0.35 w/c. As the PCE-based HRWR contents increased to 0.18% (by mass of cement), the plastic viscosity and dynamic yield stress were decreased up to 30% and 50%, respectively. The supplementary cementitious materials (SCMs) also showed significant influence on the rheological properties of UHPC pastes. Jing et al. [33] uncovered the effect of fly ash in UHPC with 0.18 w/b. As fly ash contents increased from 0 to 40%, the consistency coefficient (i.e., the linear term in the Herschel-Bulkley model) was decreased by over 85%. Li et al. [34] showed that, as the metakaolin contents increased from 0 to 8%, the dynamic yield stress was increased by 550% and the plastic viscosity was increased by 40%. The utilization of SCMs also enhances the thixotropic properties. For instance, Assaad and Khayat [26] studied the thixotropy of two mortars with different binder systems and a fixed w/b of 0.4. Compared to the mortar made with 100% cement in the binder system, the thixotropy (i.e., evaluated by the structural breakdown area) of the mortar made with 72% cement, 22% fly ash, and 6% silica fume in the binder system was increased by 50%. However, the chemical and physical properties of SCMs from different sources might be significantly different [3], which leads to inconsistent findings on the effect of SCMs on the rheological properties of cement-based materials

In order to more efficiently enhance the rheological properties of cement-based materials, viscosity-modified admixtures (VMAs) were widely utilized and investigated [36-39]. In general, VMAs are classified as organic and inorganic types. The organic VMAs are mainly composed of polymer coils, such as welan gum and diutan gum. The underlying mechanism of organic VMAs to enhance the rheological properties of UHPC pastes is that the polymer coils can interpenetrate and entangle to form networks with attractive interactions in pore solutions [36]. For instance, Teng et al. [39] found that, as welan gum contents increased from 0 to 0.09% for UHPC mortars with w/b of 0.20, the dynamic yield stress was increased by 315% and the thixotropy (i.e., evaluated by the growth rate of static yield stress) was increased by 240%. Compared to the aforementioned impact factors (i.e., w/b and SCMs addition), the addition of organic VMAs is more efficient and straightforward to adjust the rheological properties of UHPC. However, the addition of polymeric (i.e., organic) VMAs might increase the distance between cementitious particles and slow down the nucleation of hydration by decreasing the number of pseudo-contract points [36]. The retarded hydration can delay the development of mechanical strength for UHPC pastes, especially at early ages.

The inorganic VMA (i.e., nanoclay) is currently regarded as one of the most effective chemical admixtures to control the rheological properties of cement-based materials [40-42]. Several advantages of nanoclay are highlighted: (1) with high surface areas, nanoclay particles possess high water absorption to accelerate the flocculation [43]; (2) with negative surface charges, nanoclay particles have a high affinity to connect with cement particles, resulting in quick and reversible flocculation [44]; (3) with high aluminates amount, nanoclay alters the sulfate-aluminate balance in the solution, promoting the hydration of C₃A to generate more ettringite which forms the irreversible chemical connections between particles [36]; (4) with nano-sized particles, nanoclay provides extra nucleation sites to promote the formation of C—S—H [39]. The only concern is the compatibility between the type of nanoclay and PCE-based nanoclay because the interaction between PCEbased HRWR and nanoclay might diminish the effect of nanolcay enhancement on rheological properties. For instance, Lei and Plank [45] reported that the Na⁺ montmorillonite clay is incompatible with PCEbased HRWR because the adsorption rate of the Na⁺ montmorillonite clay is around 225 mg/g PCE-based HRWR. However, Qian and Schutter [44] reported that the magnesium alumina silicate nanoclay is compatible with PCE-based HRWR because adsorption rate is approximately 22 mg/g PCE-based HRWR which is acceptable. For UHPC pastes with high HRWR content, the compatibility between type of nanoclay and type of HRWR should be investigated.

In addition, the incorporation of nanoclay particles can generally lead to a significant jump in the initial static yield stress by the flocculation by electrostatic attraction forces. Afterward, the static yield stress gradually increases with the lower increasing rate of the promoted hydration [36]. Typically, the magnesium alumina silicate nanoclay powder is utilized and its shape is a needle-like structure with an approximate length and diameter of 1.75 µm and 30 nm [43,44,46–48]. Teng et al. [39] revealed that, for UHPC mortars with w/b of 0.20, as nanoclay contents increased from 0 to 0.4%, the dynamic yield stress was increased by 325% and the thixotropy (i.e., evaluated by the growth rate of static yield stress) was increased by 200%. In addition, the peak time of hydration heat for investigated UHPC mortars was accelerated by 1.5 h. It was validated that the addition of nanoclay efficiently enhanced the rheological properties of UHPC mortars and promoted its hydration as well.

Apart from the materials point of view, the rheological properties of cement-based materials are also sensitive to the change in temperatures [49–51]. Al-Martini and Nehdi [52] found that, as ambient temperature increased from 20 °C to 45 °C, the dynamic yield stress was increased by 670% and the plastic viscosity was increased by 500% for cement pastes with a fixed 0.35 w/b. Besides, Huang et al. [49] proposed that thixotropy is also sensitive to ambient temperatures. As the ambient temperatures increased from 10 °C to 40 °C, the thixotropy (i.e., evaluated by the growth rate of the static yield stress) of cement pastes with 0.30 w/c was increased by 420%. The in-site UHPC construction is under different temperatures which cannot be ignored.

However, to well disperse the traditional powder type nanoclay particles in cementitious suspension is reported challenging, especially on job sites. Due to the nano size, any agglomeration becomes notable and highly compromises their reinforcing performance [53,54]. The traditional dispersion methods, such as ultra-sonification technology [55] and surfactants technology [56], are only available in the lab experiments but hard to apply for large-scale UHPC production on job sites. Therefore, in this study, a well-dispersed water-based nanoclay suspension is first utilized. Moreover, there is a lack of knowledge on the coupled effect of water-based nanoclay suspension and ambient temperature on the rheological properties of UHPC pastes to date.

To address the problems mentioned above, comprehensive laboratory experiments were conducted and five water-based nanoclay suspension contents (from 0 to 0.20%) and three ambient temperatures (e. g., 10 $^{\circ}$ C, 25 $^{\circ}$ C, and 35 $^{\circ}$ C) were designed to elaborate the coupled effects on rheological properties of UHPC pastes. This research has four

Table 1Chemical and physical properties of raw materials.

	Type I cement	Slag	Nanoclay
SiO ₂ (%)	22.44	36.21	55.20
Al ₂ O ₃ (%)	2.76	11.10	12.20
Fe ₂ O ₃ (%)	2.24	0.76	4.05
CaO (%)	68.05	43.75	1.98
MgO (%)	0.91	5.09	8.56
SO ₃ (%)	2.25	2.21	-
Na ₂ O (%)	0.19	0.23	0.53
K ₂ O (%)	0.11	0.40	0.68
TiO ₂ (%)	0.14	0.58	0.49
P ₂ O ₅ (%)	0.09	0.02	0.65
Mn ₂ O ₃ (%)	0.03	0.36	-
C ₃ S (%)	50.51	_	-
C ₂ S (%)	23.32	_	-
C ₃ A (%)	11.42	_	_
C ₄ AF (%)	6.12	_	_
Loss of ignition (%)	1.28	0.72	15.66
Specific gravity (g/cm ³)	3.15	2.9	1.14

Table 2 Mixture design (kg/m³).

Mixtures	Cement	Slag	HRWR	Water	Nanoclay
Ref	745.6	1029.6	11.0	400.8	0
NC-0.05%	745.6	1029.6	11.0	397.1	4.6
NC-0.10%	745.6	1029.6	11.0	393.5	9.1
NC-0.15%	745.6	1029.6	11.0	389.8	13.7
NC-0.20%	745.6	1029.6	11.0	386.1	18.2

Note: HRWR represents a high-range water reducer.

objectives: (1) to validate the compatibility between the new water-based nanoclay with common-used PCE-based HRWR; (2) to evaluate the effect of nanoclay contents and ambient temperature on dynamic yield stress and plastic viscosity of UHPC pastes with w/b of 0.23; (3) to evaluate the effect of nanoclay contents and ambient temperature on the thixotropy of UHPC pastes with w/b of 0.23, including initial fluctuations of static yield stress ($\tau_{\rm floc}$) and thixotropy index (I_A); (4) to understand and elaborate the underlying mechanisms and key components that enhances the rheological properties of UHPC pastes. This research will advance the application of the water-based nanoclay suspension to tailor the UHPC with adapted rheological properties under different ambient temperatures.

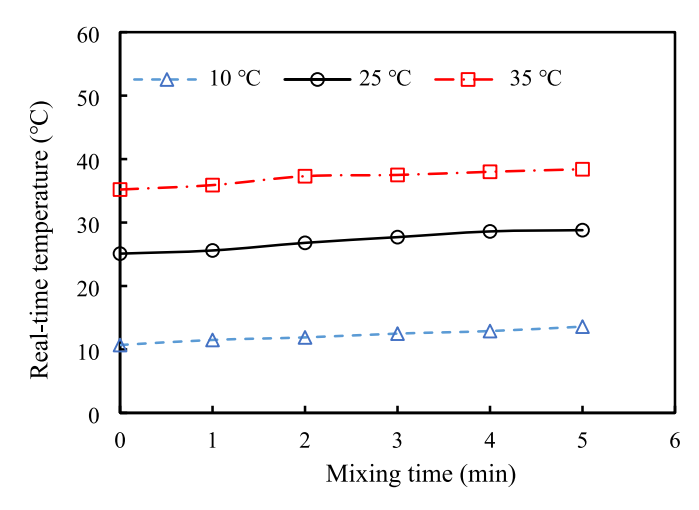
2. Materials, mixture designs, and mixing procedures

2.1. Raw materials

Type I Portland cement and slag from a local plant in New Jersey were employed as binders. A new type of water-based magnesium alumina silicate nanoclay suspension in gray color was applied for the first time. Based on the patented production process, the surface of nanoclay is negatively charged owing to the substitution of Al³⁺ or Mg²⁺ ions with silicon [57]. The solids content, specific gravity, and pH values of the nanoclay suspension are 19.5%, 1.14, and 8.5, respectively. Besides, the viscosity of the nanoclay suspension is 100 centipoise and the residue of 45-µm mesh is lower than 0.01%, indicating the good dispersion of nanoclay powder. No extra dispersion technology needs to apply during the utilization process. The chemical compositions and physical characteristics of all materials were listed in Table 1. To maintain excellent workability, a polycarboxylate (PCE)-based high-range water reducer (HRWR) was used. The solid content and specific gravity were 34.4% and 1.05.

2.2. Mixture designs

The reference UHPC paste (i.e., Ref) is consist of 60% slag and 40%



 $\begin{tabular}{lll} Fig. & 1. & Measured & temperature & of & UHPC & pastes & at & different & mixing \\ temperatures. & \\ \end{tabular}$

cement by volume of binder. The water-to-binder ratio (w/b) was fixed at 0.23 and the dosage of liquid high-range water reducer (HRWR) was 0.62%, both by mass of binder. In this study, the mass of PCE-based HRWR is the mass in liquid form sold by the supplier. The nanoclay contents were 0.05%, 0.10%, 0.15%, and 0.20%, by mass of binder. All the mixture designs are listed in Table 2. Besides, the effect of ambient temperature was also studied. Three ambient temperatures were considered in this study, including $10\,^{\circ}\text{C}$, $25\,^{\circ}\text{C}$, and $35\,^{\circ}\text{C}$.

2.3. Mixing procedures

Three different temperature levels were considered in this study, which are 10 °C, 25 °C, and 35 °C, simulating field production of UHPC at different seasons. For each temperature, the raw materials, and apparatuses in direct contact with mixtures, such as the mixing bowl and paddle, were stored in an environmental chamber for 5 h before the mixing to ensure the starting temperature of the mixture is consistent with the target temperature. Afterwards, the Hobart N50 mixer was employed to prepare UHPC pastes as follows: (1) Step 1: the dry ingredients (cement and slag) were introduced to the mixer and mixed at 1 rps for 1 min; (2) Step 2: the weighed water-based nanoclay and HRWR were dissolved in the mixing water; (3) Step 3: the 90% of the dissolved solution (including mixing water, nanoclay, and HRWR) was introduced to the mixer and mixed at 1 rps for 2 min; (4) Step 4: The rest of dissolved solution was added to the mixer and mixed at 2 rps for 1 min. The total mixing time of UHPC pastes was 5 min.

In addition, considering that the friction between particles with mixing paddle might affect the final temperature of UHPC pastes, the temperature evolution during the mixing process was measured, as shown in Fig. 1. Results showed that the temperature increment is lower than 4 $^{\circ}$ C, which shows limited effect.

3. Experimental methods

3.1. Total organic carbon (TOC) test

The adsorption of high-range water reducer (HRWR) on particles or agglomerates of cementitious materials or nanoclay is evaluated by the total organic content of carbon in pore solution of UHPC pastes [44,58]. In order to minimize the effects from the hydration products, the sample preparation was carried out right after the mixing process. Specifically, the fresh UHPC pastes were filled in the plastic tubes and centrifuged at 10,000 RPM for 5 min to separate into the supernatant pore solution and the solid precipitations. Subsequently, the supernatant on the top was extracted with a syringe and filtered through 0.45 µm polyether sulfone

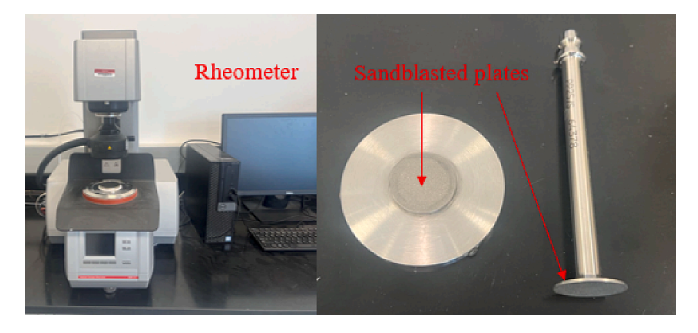


Fig. 2. The rheology test equipment: Anton Paar MCR 302 rheometers.

membrane. To remove the inorganic carbon, 2% nitric acid is added into the pore solution. Finally, the solution is analyzed with the TOC analyzer. Four samples were analyzed, including pure HRWR, Ref, NC-0.10%, and NC-0.20%.

3.2. Workability

According to ASTM C230/C230M [59], the mini-slump flow spreads were measured to evaluate the workability of UHPC pastes. After the mixing process, all homogenized UHPC pastes were rested for 2 min to minimize the effect of mixing and vibration history. The fresh UHPC pastes were poured into the slump cone and the cone was gradually lifted. Finally, the diameters of the fresh UHPC were measured. All measurements were repeated three times to secure the reproductivity of the results.

3.3. Rheology measurements and thixotropy evaluation

The Anton Paar MCR 302 rheometer was applied to evaluate the rheological properties of UHPC pastes, as shown in Fig. 2. Previous research found out that the rheology of cement-based materials with low w/b would significantly enhance with the increase of the temperature and time [49]. In order to protect the equipment from being damaged

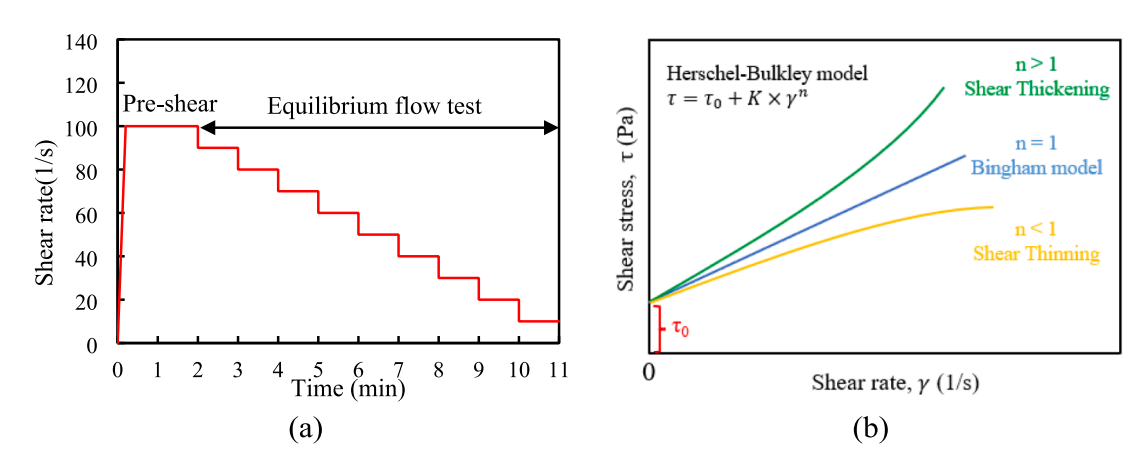


Fig. 3. The protocol to determine dynamic yield stress and plastic viscosity: (a) equilibrium flow curve (b) the Bingham model.

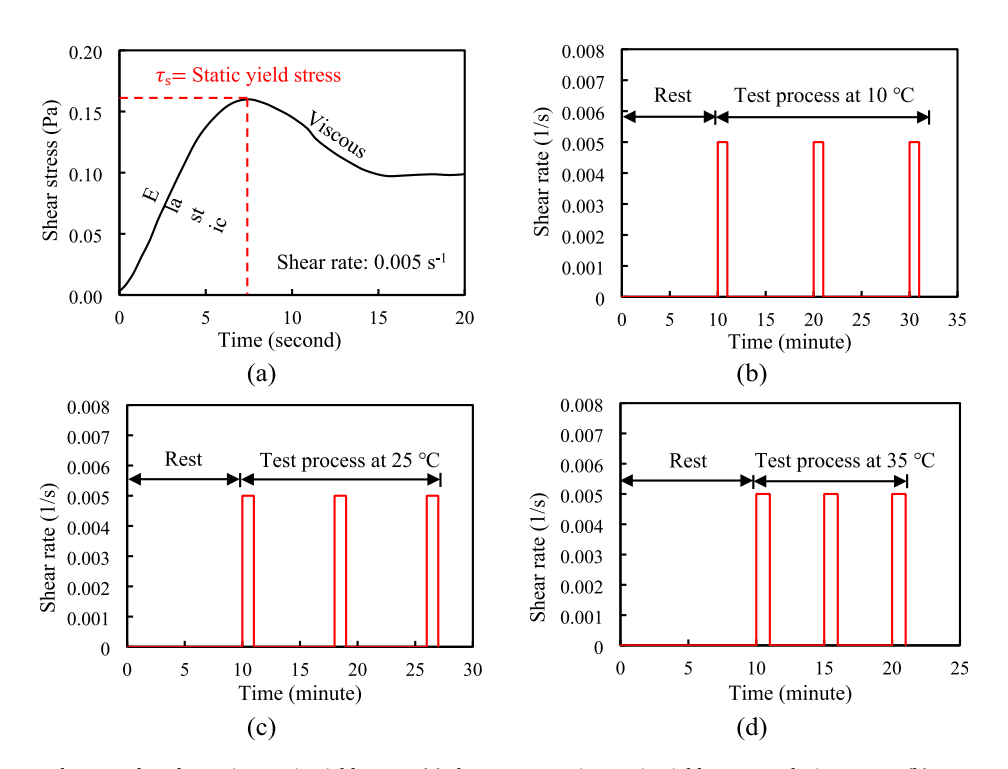


Fig. 4. The shear-rate-control protocol to determine static yield stress: (a) the representative static yield stress evolution curve; (b) test protocols at 10 °C; (c) test protocols at 25 °C; and (d) test protocols at 35 °C.

due to the overload, the plate-type measurement probe was selected in this study. The sandblasted plates are 25 mm in diameter, which can minimize the slip between the plate and fresh UHPC paste samples.

3.3.1. Protocol to determine dynamic yield stress and plastic viscosity

The fluid can be generally divided as Newtonian fluid and Non-Newtonian fluid. Since the UHPC pastes are composed of high-volume solid cementitious materials with different particle size distributions, chemical admixtures, and low free water, the UHPC pastes are commonly regarded as Non-Newtonian fluid [60,61]. Detail procedures to evaluate the rheological properties of UHPC pastes were introduced below: (1) Step 1: the UHPC pastes were pre-shared at 100 s⁻¹ for 2 min; (2) Step 2: the shear rate was stepwise from 100 s^{-1} to 10 s^{-1} . For each step, the shear rate was kept for 1 min (Fig. 3(a)); (3) Step 3: the steadystate of the shear stress was fitted by the Herschel-Bulkley model (Fig. 3 (b)). In this model, the fresh UHPC pastes begins to flow as the shear stress surpass the critical scraping stress limitation, and its strain gradient increases with the power increment. The equation of the Herschel-Bulkley model is shown in Eq. (1). However, the Herschel-Bulkley model does not directly give the plastic viscosity of the UHPC paste. Hu and De Larrard [60] derived the empirical formulas to calculate the plastic viscosity through the parameters from Herschel-Bulkley model, shown in Eq. (2). To be noted, the rheological experimental measurement was conducted after the mixing procedures.

$$\tau = \tau_0 + K \times \gamma^n \tag{1}$$

$$\mu = \frac{3 \times K}{n+2} \times \gamma_{max}^{n-1} \tag{2}$$

where τ represents the shear stress (Pa), τ_0 represents the dynamic yield stress (Pa), K represents the consistency (Pa·sⁿ), γ represents the shear rate (1/s), and n represents the flow index (unitless). As the n < 1, the fresh UHPC paste shows the shear thinning property; as the n = 1, the fresh UHPC paste conforms to the Bingham model; as the n > 1, the fresh UHPC paste shows the shear thickening property. μ represents the plastic viscosity, γ_{max} represents the maximum shear rate during the rheological tests.

3.3.2. Protocol to determine static yield stress

The static yield stress is sensitive to the shear history, the mixing regime, and the rest time [62]. Thus, the initial static yield stress right after the mixing procedures was extremely low. The initial static yield stress was considered equal to the dynamic yield stress at this time instant. Afterward, the static yield stress of fresh UHPC pastes was tested based on the shear-rate-control method, as shown in Fig. 4(a). The first measurement was conducted 10 min after the mixing procedures. During the test, UHPC pastes were subjected to a very low shear rate for 1 min without any pre-shear. Based on the recommendation from Yuan et al. [62], the shear rate of 0.005 s $^{-1}$ was selected.

Preliminary studies showed that the ambient temperatures have significant effects on the development of the static yield stress, thus the time gap between testing for different ambient temperatures was slightly different to ensure that the collected data are in the proper range: (1) when the ambient temperature was 10 °C, the time gap between testing was 10 min (i.e., the static yield stress test was conducted at 10 min, 20 min, and 30 min, as shown in Fig. 4(b)); (2) When the ambient temperature was 25 °C, the time gap between testing was 8 min (i.e., the static yield stress test was conducted at 10 min, 18 min, and 26 min, as shown in Fig. 4(c)); (3) when the ambient temperature was 35 °C, the time gap between testing was 5 min (i.e., the static yield stress test was conducted at 10 min, 15 min, and 20 min, as shown in Fig. 4(d)).

3.3.3. Evaluation of thixotropy

The thixotropy of UHPC pastes was evaluated by the evolution of the static yield stress, as shown in Fig. 5. This evaluation method was

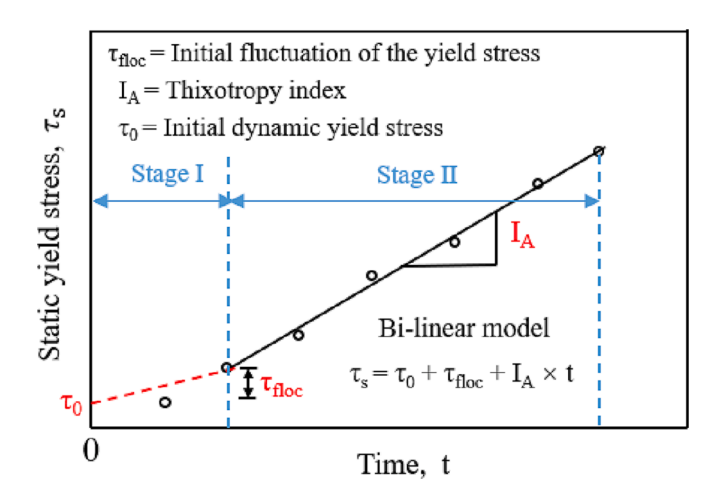


Fig. 5. Evaluation of thixotropy of UHPC pastes.

proposed by Mostafa and Yahia [63], Roussel [64], and Teng et al. [39]. The evolution of the yield stress can be fitted by a bi-linear model proposed by Kruger et al. [65], as shown in Eq. (3). The bi-linear model divided the whole process into two stages with different fitting slopes. However, it is worth noting that the model is only suitable to describe the thixotropy of cement pastes within one hour since the exponential evolution of the static yield stress with time can take place after one hour [66].

$$\tau_s = \tau_0 + \tau_{floc} + I_A \times t \tag{3}$$

where τ_s is the static yield stress at the corresponding time, t is the time starting from when the mixing procedures were done, I_A is the thixotropy index, τ_0 is the dynamic yield stress, and τ_{floc} is the initial increase between dynamic yield stress and static yield stress.

3.4. Isothermal calorimetry

The rate of hydration was evaluated by using an isothermal calorimeter (Calmetrix I-Cal 4000 HPC), which was programmed to maintain the samples at 10° C, 25° C, and 35° C. About 60 g of fresh UHPC pastes was sealed in a plastic vial and placed into the calorimeter. The heat of hydration data was measured 2 min after mixing process and continuously measured for the next 36 h. The results were normalized by the mass of the binder.

3.5. X-ray diffraction (XRD) analysis

A solvent exchange method with isopropanol was adopted to stop the hydration of fresh UHPC pastes at different time instants to investigate the development of hydration process [67]. Specifically, about 10 mL of fresh UHPC pastes after specific time instant (i.e., 0 min, 15 min, and 30 min) was filled in a 50 mL tube and centrifuged at 10,000 RPM for 5 min. Then, the supernatant water was removed. About 40 mL of isopropanol was added into the tube. The tube was shaken for 1 min for the homogenization. Subsequently, the sample was centrifuged again at 10,000 RPM for 5 min. In addition, the solvent exchange method procedures were repeated once. The final UHPC pastes were drying in a ventilated oven for 15 min at 40 $^{\circ}$ C, and then for 2 days in a desiccator over silica gel and soda lime to minimize carbonation.

The phase change of UHPC pastes were analyzed by XRD test. The X-ray diffraction test was carried out using a diffractometer (model: Panalytical X' pert Pro) to evaluate the hydration products of the mixtures. The sample preparation was introduced before. During the XRD test, powder samples were scanned on a rotating stage between $5\circ$ and $65\circ$ (2θ) using an X'Celerator detector. The step size of scanning was $0.0167\circ(2\theta)$, and the time per step was 30 s. Finally, XRD coupled with

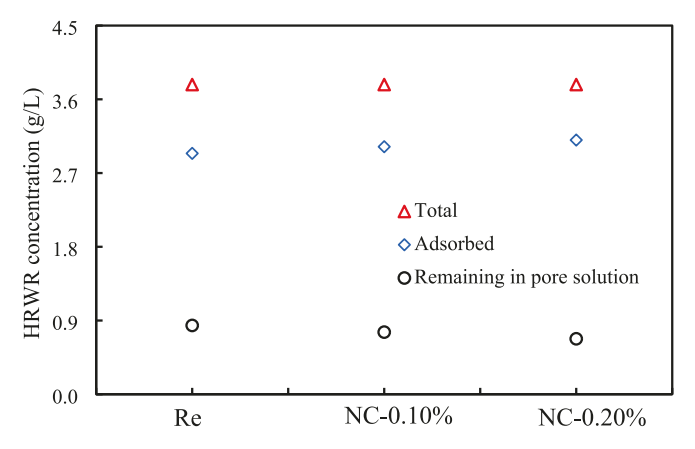


Fig. 6. PCE-based HRWR of total content, adsorbed on all particles (including cement, slag, and nanoclay), and remaining in pore solution.

Rietveld refinements was employed to quantify the phase assemblage in the UHPC paste samples [68].

3.6. Scanning electron microscopy (SEM)

The pictures of UHPC pastes at different stages of hydration were observed by SEM. The SEM was conducted using the microscope (model: Zeiss Auriga FIB/SEM with a SE2 detector) operated in secondary electron detection mode with high-vacuum and an acceleration voltage of 5 kV. The sample preparation is the same as the XRD test introduced in Section 3.5. The powder sample was placed on carbon tape attached to the sample holder. Several regions were examined to ensure the observed structures were representative.

4. Experimental results

4.1. Adsorption of PCE-based HRWR in nanoclay

Previous studies indicated that the HRWR in cement pastes are generally divided into three parts [69]: (1) consumed by the chemical hydration, in particular for the C—S—H formation; (2) adsorbed on the surface of particles or agglomerates of cementitious materials and hydration products; (3) remaining in the pore solution. In order to minimize the hydration reaction effects, the centrifugation step of the fresh UHPC pastes was conducted immediately after the mixing process. In this case, the majority of HRWR would be either absorbed on the surface of cementitious materials or remained in the pore solution. Besides, the polyethylene oxide (PEO) side chains of the PCE based HRWR could also chemically adsorb or intercalate into the layers of the aluminosilicate and physically adsorb on the negatively charged surface of the nanoclay [45,70]. Therefore, the PCE-based HRWR might be trapped in nanoclay networks as well.

The total organic carbon (TOC) analysis was carried out to investigate the adsorption of PCE-based HRWR on nanoclay in this research because the strong intercalation between HRWR and nanoclay would significantly diminish the dispersing effect of HRWR in cement-based materials [45]. Fig. 6 summaries the HRWR concentration of total, adsorbed, and remaining in pore solution. Specifically, the total HRWR concentration is the constant value (i.e., $11.0 \times 0.344 = 3.78$), the remaining HRWR concentration is measured from the total organic carbon (TOC) test, and the adsorbed value is the total value subtracts the remaining content. Results indicated that, as the nanoclay content increased from 0 to 0.20%, the remaining PCE-based HRWR decreased from 0.84 g/L to 0.67 g/L (by 20%). Thus, the adsorbed amount of PCE-based HRWR linearly increases with the nanoclay addition. In this study, the adsorption rate of the nanoclay is calculated as 47.9 mg/g of HRWR. Compared to the previous research [44,45], the adsorption rate of the

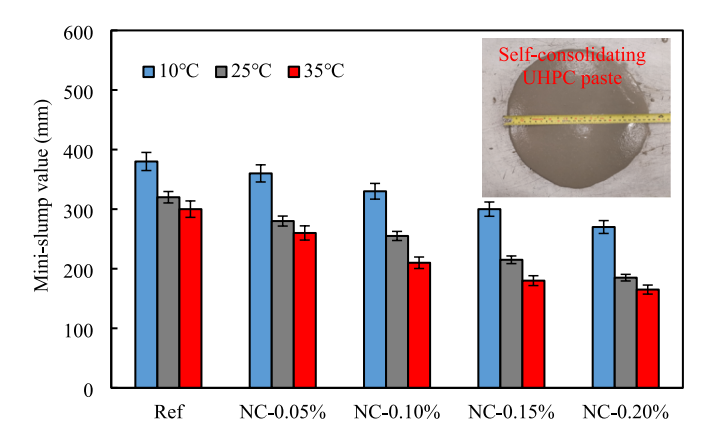


Fig. 7. Results of mini slump spread for investigated UHPC pastes.

PCE-based HRWR by the water-based nanoclay is low. Therefore, it could be reasoned that the water-based nanoclay has good compatibility with PCE-based HRWR in this study.

4.2. Workability

The workability of cement-based materials is closely related to construction quality. Poor workability might result in poor compaction and difficult placement [71]. Thus, the effect of nanoclay contents and ambient temperatures on the workability of fresh UHPC pastes was investigated. Fig. 7 plots mini slump spread results of investigated UHPC pastes with nanoclay contents (e.g., 0–0.20%) at ambient temperatures (e.g., 10 °C, 25 °C, and 35 °C). Overall, the fresh UHPC pastes are self-consolidating and mini-slump spreads decrease with the increase of nanoclay contents and ambient temperatures.

As the nanoclay content increased from 0 to 0.20%, the mini-slump spreads were reduced by 20%, 45%, and 50% for investigated UHPC pastes at 10 °C, 25 °C, and 35 °C, respectively. The effect of nanoclay can be attributed to: (1) the nanoclay particles have high capacity to absorb free water for lubrication [72]; (2) the cement and slag particles are attracted by the nanoclay particles by the electrostatic attraction forces to accelerate the flocculation [43]; (3) the addition of nanoclay traps a small amount of HRWR to diminish the positive effect of HRWR. In addition, as the ambient temperatures increased from 10 °C to 35 °C, the mini-slump spread values were reduced by 21%, 28%, 36%, 40%, and 39% for the mixture of Ref, NC-0.05%, NC-0.10%, NC-0.15%, and NC-0.20%, respectively. The effect of ambient temperature can be attributed to that the higher ambient temperature promotes the dissolution of cement and slag particles and exacerbates the Brownian motion of the particles (i.e., random thermal motion of particles) to accelerate the quick flocculation, resulting in the reduction of the workability of UHPC pastes. The coupled effect of higher ambient temperature and the addition of nanoclay could significantly undermine the workability of UHPC pastes.

4.3. Dynamic yield stress and plastic viscosity

The rheological properties of UHPC pastes include dynamic yield stress and plastic viscosity. The dynamic yield stress is the minimum stress required for maintaining flowable status, and lower dynamic yield stress generally corresponds to better workability (i.e., higher minislump spreads) [73]. The plastic viscosity is the resistance offered by fresh UHPC pastes to flow freely, and proper plastic viscosity is generally required to secure good fiber dispersion and orientation [2]. Therefore, the coupled effect of nanoclay contents and ambient temperature on dynamic yield stress and plastic viscosity needs to be clarified.

Fig. 8(a) to 8(c) plots the equilibrium flow curves of UHPC pastes with different nanoclay contents (e.g., 0–0.20%, by mass of binder) at

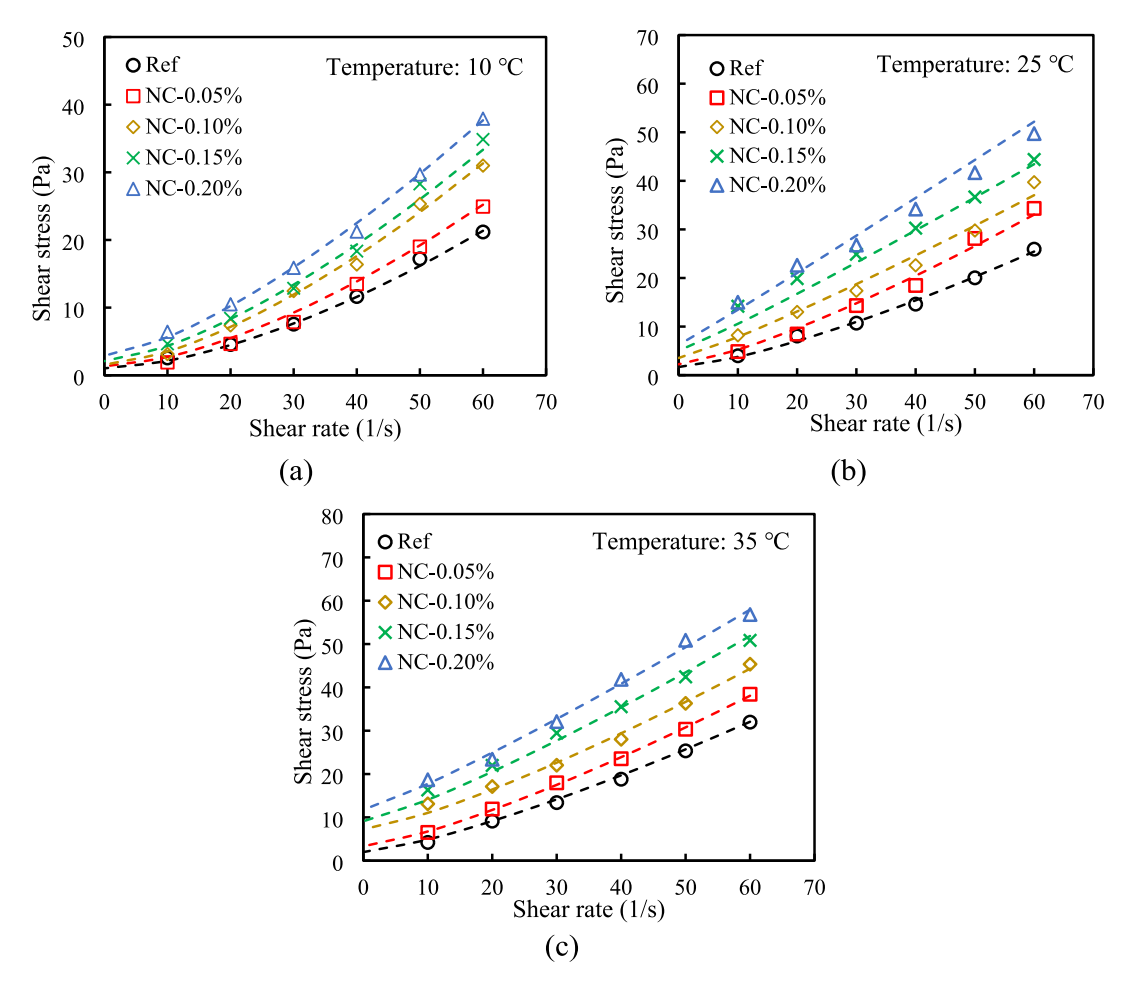


Fig. 8. Results of equilibrium flow curves for UHPC pastes: (a) 10 $^{\circ}$ C; (b) 25 $^{\circ}$ C; and (c) 35 $^{\circ}$ C.

different ambient temperatures (e.g., $10\,^{\circ}$ C, $25\,^{\circ}$ C, and $35\,^{\circ}$ C). All data points were fitted by the Herschel-Bulkley model and results of each parameter were shown in Table 3.

Fig. 9(a) and 9(b) summarize the results of dynamic yield stress and plastic viscosity for UHPC pastes based on the Herschel-Bulkley model. As the nanoclay content increased from 0 to 0.20%, the dynamic yield stresses were increased by 180%, 270%, and 490% at 10 °C, 25 °C, and 35 °C, and the plastic viscosity were increased by 80%, 110%, and 65% at 10 °C, 25 °C, and 35 °C. The results showed the nanoclay can efficiently enhance the rheological properties of UHPC pastes. Notably, the development of dynamic yield stress (by 200% ~ 500%) was much faster than that of plastic viscosity (by $60\% \sim 110\%$). The enhancement of the rheological properties by adding nanoclay can be attributed to (1) physical effect: the cement and slag particles are attracted by the nanoclay particles by the electrostatic attraction forces, thus increasing the minimum stress required for maintaining the flow state [43]; (2) chemical effect: nanoclay with high aluminates alters the sulfatealuminate balance in the solution, resulting in the secondary hydration of C₃A. The reduced free mixing water and newly formed ettringite increase the minimum stress required for flowable state [74].

As the ambient temperatures increased from 10 °C to 35 °C, the dynamic yield stresses were increased by 95%, 150%, 360%, 330%, and 320% for Ref, NC-0.05%, NC-0.10%, NC-0.15%, and NC-0.20% and the plastic viscosity were increased by 62%, 58%, 34%, 48%, and 44%. The results showed that the rise of ambient temperatures can efficiently increase the rheological properties of UHPC pastes. Similarly, the development of dynamic yield stress (by 100% \sim 350%) was much faster than that of plastic viscosity (by 35% \sim 65%). The enhancement of the rheological properties by ambient temperatures also can be attributed to

two reasons: (1) physical effect: higher ambient temperature promotes the dissolution of cement and slag particles and exacerbates the Brownian motion of the all particles to accelerate the flocculation; (2) the chemical effect: higher ambient temperature promotes the initial hydration process [49]. In summary, the nanoclay is a promising chemical admixture to efficiently enhance the dynamic yield stress and plastic viscosity of UHPC pastes. Besides, under the coupled effect of ambient temperatures, the effect of nanoclay on rheological properties can be further enhanced.

Besides, the correlation between the mini-slump spreads and dynamic yield stress was found shown in Fig. 10 based on the experimental results. Regardless of the change of ambient temperatures, an exponential relationship was established. The findings indicated that the mini-slump spreads can be used as a simple and reliable indicator for the dynamic yield stress of UHPC pastes.

4.4. Static yield stress and thixotropy evaluation

As introduced in Section 3.2.3, the evolution of the static yield stress was used to evaluate the thixotropy. The static yield stress is the minimum stress for initiating the flowable status. To measure the static yield stress, the shear-rate-control method was applied. All shear stress-shear time curves for Ref, NC-0.05%, NC-0.10%, NC-0.15%, and NC-0.20% at different ambient temperatures (e.g., 10 °C, 25 °C, and 35 °C) were plotted in Fig. A1 in Appendix. Among shear stress-shear time curves, the peak values of the shear stress for each curve refer to the static yield stress at corresponding time instants. Meanwhile, the initial static yield stress was considered equal to the initial dynamic yield stress. Fig. 11(a), Fig. 11(c), and Fig. 11(e) plot the bi-linear relationships of static yield

Table 3 Fitting parameters of the Herschel-Bulkley model.

Temp	Mixtures	Consistency, K, (Pa·s ⁿ)	Flow index, n, (unitless)	Dynamic yield stress, τ_0 , (Pa)	Plastic viscosity, μ, (Pa·s)
NC- 0.09 NC- 0.10 NC-	Ref	0.027	1.614	1.021	0.281
	NC- 0.05%	0.036	1.587	1.312	0.333
	NC- 0.10%	0.059	1.519	1.544	0.423
	NC- 0.15%	0.077	1.466	2.087	0.451
	NC- 0.20%	0.102	1.412	2.872	0.510
25 °C	Ref	0.092	1.355	1.672	0.354
	NC- 0.05%	0.153	1.295	2.235	0.468
	NC- 0.10%	0.314	1.14	3.528	0.534
	NC- 0.15%	0.461	1.08	5.020	0.624
	NC- 0.20%	0.677	1.033	6.210	0.758
35 °C	Ref	0.143	1.305	1.987	0.455
	NC- 0.05%	0.174	1.293	3.321	0.528
	NC- 0.10%	0.223	1.256	7.210	0.568
	NC- 0.15%	0.314	1.221	9.112	0.668
	NC- 0.20%	0.433	1.144	11.751	0.735

Note: The minimum R² is 0.98 for the fitting results by Herschel-Bulkley model.

stress over test time at 10 °C, 25 °C, and 35 °C. The difference between the initial static yield stress (i.e., dynamic yield stress) after mixing procedures and the static yield stress at 10 min refers to the initial fluctuation of the yield stress (τ_{floc}). The fitting line slopes of the static yield stress development refers to the thixotropy index (I_A): (1) the slopes of the static yield stress development from 10 mins to 30 mins for UHPC pastes at 10 °C; (2) the slopes of the static yield stress development from 10 mins to 26 mins for UHPC at 25 °C; and (3) the slopes of the static yield stress development from 10 mins to 20 mins at 35 °C. Fig. 11(b), Fig. 11(d), and Fig. 11(f) summarize the initial fluctuation of yield stress (τ_{floc}) and thixotropy index (I_A) at 10 °C, 25 °C, and 35 °C.

When the ambient temperature was at 10 °C, as the nanoclay content increased from 0 to 0.20%, the initial fluctuation of the static yield stress ($\tau_{\rm floc}$) was ranged from 0.7 Pa to 2.8 Pa and the thixotropy index (I_A) was ranged from 0.1 Pa/min to 3.2 Pa/min. When the ambient temperature was at 25 °C, as the nanoclay content increased from 0 to 0.20%, the initial fluctuation of the static yield stress ($\tau_{\rm floc}$) was ranged from 1.2 Pa

to 27.7 Pa and the thixotropy index (I_A) was ranged from 2.0 Pa/min to 50.6 Pa/min. When the ambient temperature was at 35 °C, as the nanoclay content increased from 0 to 0.20%, the initial fluctuation of the static yield stress (τ_{floc}) was ranged from 3.1 Pa to 38.7 Pa and the thixotropy index (I_A) was ranged from 42.0 Pa/min to 545.2 Pa/min. The results showed the coupled effect of nanoclay addition and ambient temperature can significantly increase the thixotropy of UHPC pastes. The underlying mechanisms were introduced below.

In Stage I (from 0 to 10 min), the initial fluctuation of the static yield stress was affected by the physical effect and chemical effect. Meanwhile, the physical effect plays as the main contributor: (1) the nanoclay particles with negative surface charges (introduced in Section 2.1) were connected with cement and slag particles by electrostatic attraction forces to form new networks, resulting in the resistance to initiate the free flow; (2) higher ambient temperatures promoted the dissolution of cement and slag particles in the mixing water and accelerated the Brownian motions of particles, further facilitating the contact among cement, slag and nanoclay particles. In Stage II (from 10 min to 30 min), the static yield stress started to linearly increase over the test time. During this period, the evolution of the static yield stress was the sum of physical effects and chemical effects. The physical effects were still present, likewise in Stage I. In addition, the further increase of the static yield stress came from the chemical effects: (1) higher ambient temperature quickly promoted the reaction between C₃A and gypsum to generate more ettringite [75]; (2) nanoclay with high aluminates alters the sulfate-aluminate balance in the solution, resulting in secondary hydration of C₃A to generate more ettringite [74]. The coupled effect of the physical particles' flocculation and chemical hydration reaction leads to a significant increment of the static yield stress in this period,

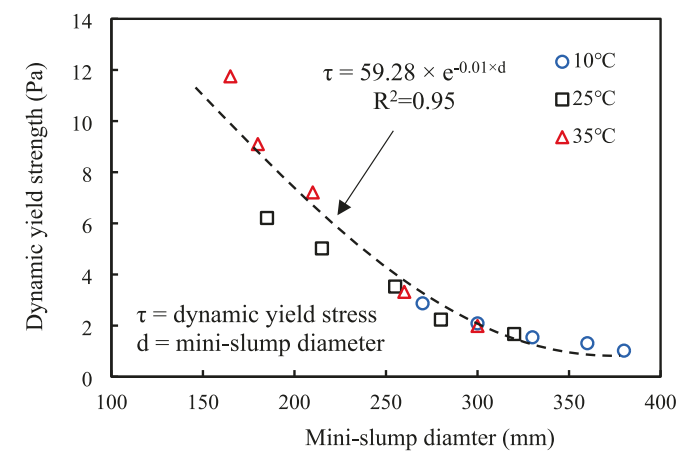
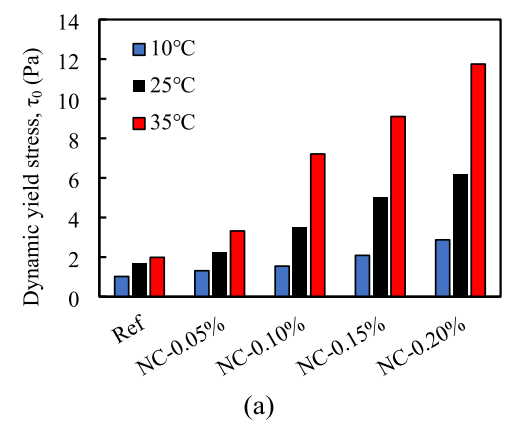


Fig. 10. Correlation between mini slump spread and dynamic yield stress.



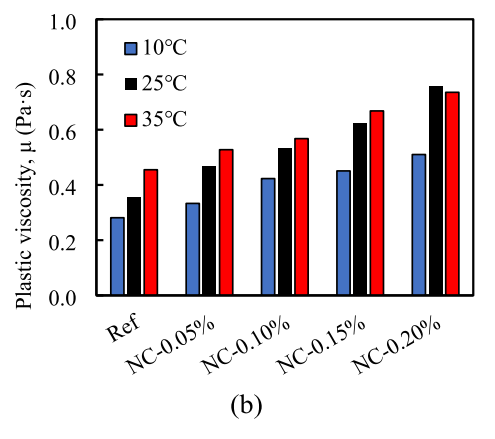


Fig. 9. Results of rheological properties: (a) dynamic yield stress; and (b) plastic viscosity.

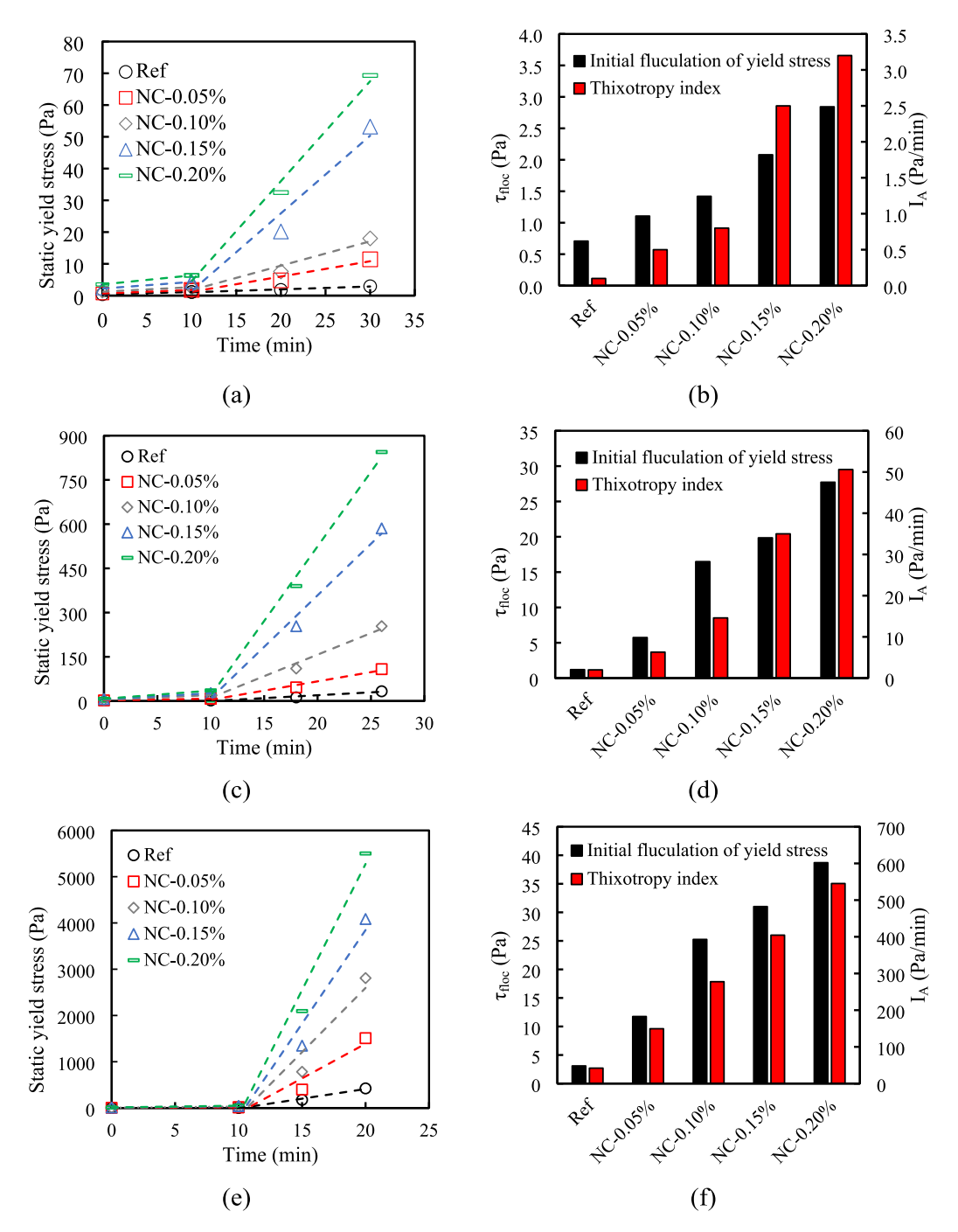


Fig. 11. The results of initial fluctuation of static yield stress (τ_{floc}) and thixotropy index (I_A): (a) the bi-linear fitting lines at 10 °C; (b) summaries of calculated results at 10 °C; (c) the linear fitting lines at 25 °C; (d) summaries of calculated results at 25 °C; (e) the linear fitting lines at 35 °C; (f) summaries of calculated results at 35 °C.

shown in thixotropy index (IA).

In summary, nanoclay is a promising admixture to enhance the thixotropy of UHPC pastes. Moreover, the effect of varying temperatures on job sites should not be ignored.

4.5. Hydration heat

The isothermal calorimeter was conducted to quantify the hydration process of UHPC pastes. To evaluate the effect of chemical hydration on rheological properties, the curves for the first hour are provided, as shown in Fig. 12(a) and 12(b).

As the nanoclay contents increased from 0 to 0.20%, the first peaks of

heat flow curves were increased by 140%, 20%, and 12% at 10 $^{\circ}$ C, 25 $^{\circ}$ C, and 35 $^{\circ}$ C. In addition, the cumulative heat within the first hour was increased by 35%, 22%, and 20% at 10 $^{\circ}$ C, 25 $^{\circ}$ C, and 35 $^{\circ}$ C. Results validated the efficient promotion of hydration by adding nanoclay. In comparison, as the ambient temperatures increased from 10 $^{\circ}$ C to 35 $^{\circ}$ C, the first peaks of heat flow curves were increased by 1200%, 900%, and 480% for Ref, NC-0.10%, and NC-0.20%. In addition, the peaks of heat flow were increased by 530%, 480%, and 460% for Ref, NC-0.10%, and NC-0.20%.

In summary, it could be reasoned that, both the high temperature and nanoclay addition promotes the chemical hydration process of UHPC pastes in the first hour, thus affecting the rheological properties of

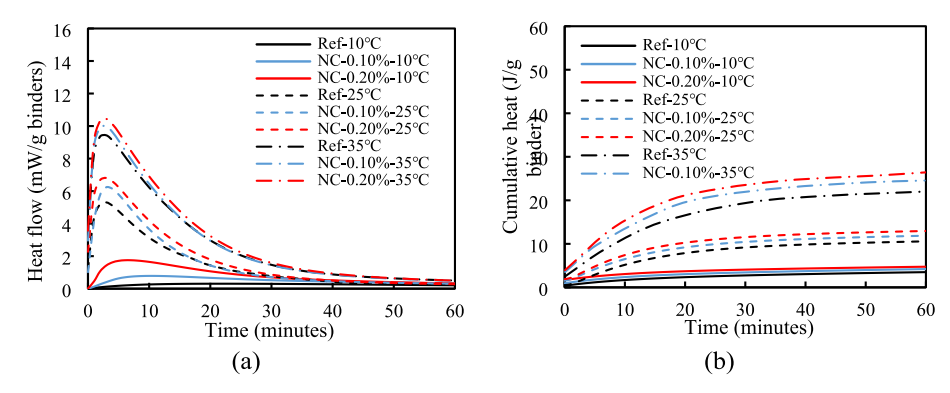


Fig. 12. Hydration heat results from UHPC pastes with nanoclay contents at different ambient temperatures: (a) the heat flow curves; and (b) the cumulative heat curves.

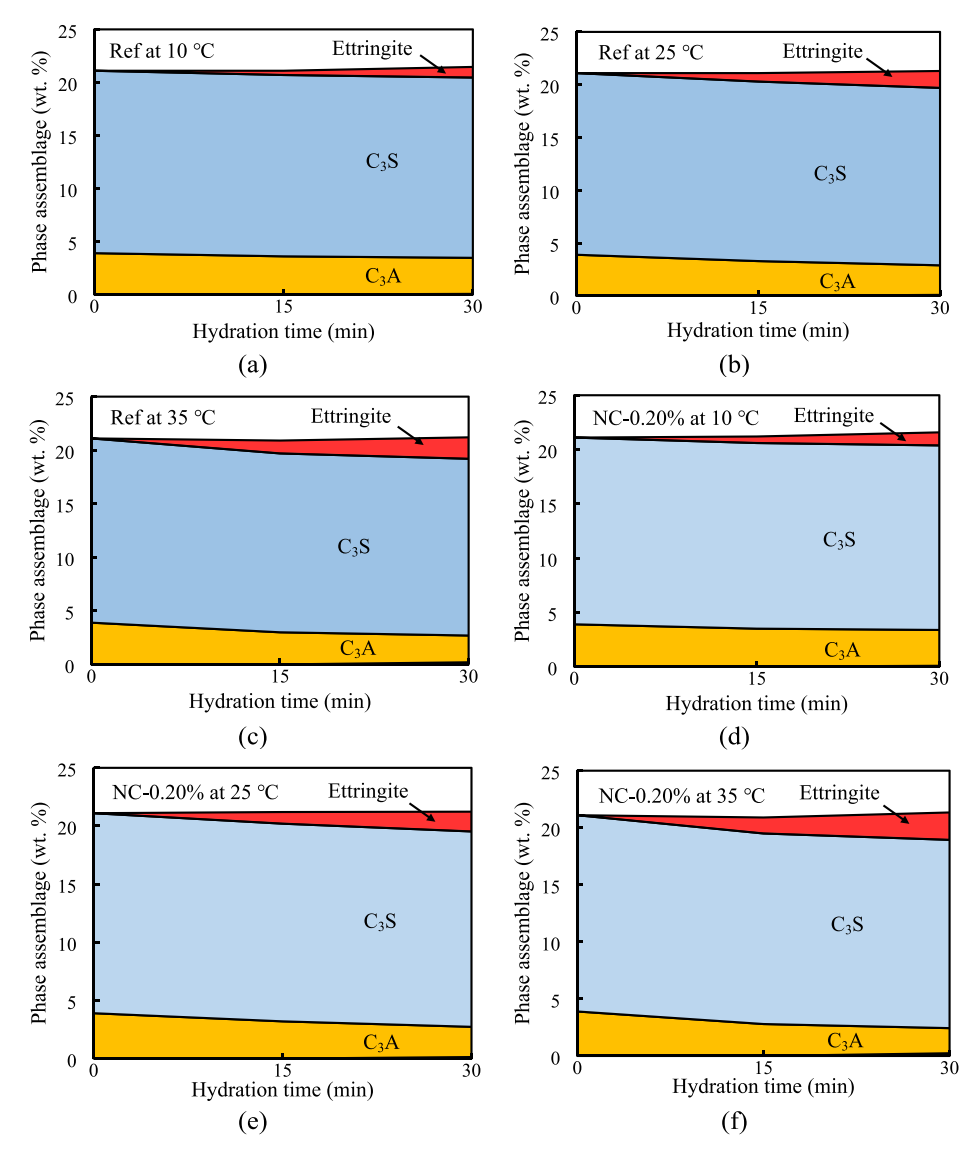


Fig. 13. Phase development of investigated UHPC pastes: (a-c) the hydration reaction for Ref within the first 30 min at 10 °C, 25 °C, and 35 °C; (d-f) the the hydration reaction for NC-0.20% within the first 30 min at 10 °C, 25 °C, and 35 °C. The given results are the average results of three independent measurements. Expected values at the mixing time: $C_3S = 17.2$ wt% and $C_3A = 3.9$ wt% (i.e., t = 0 min in this figure).

UHPC pastes. Moreover, ambient temperatures showed much more pronounced effects on promoting hydration, compared to nanoclay additions.

4.6. Quantitative XRD analysis

The XRD analysis coupled with Rietveld refinements method was employed to quantify the phase change in the UHPC paste samples [68].

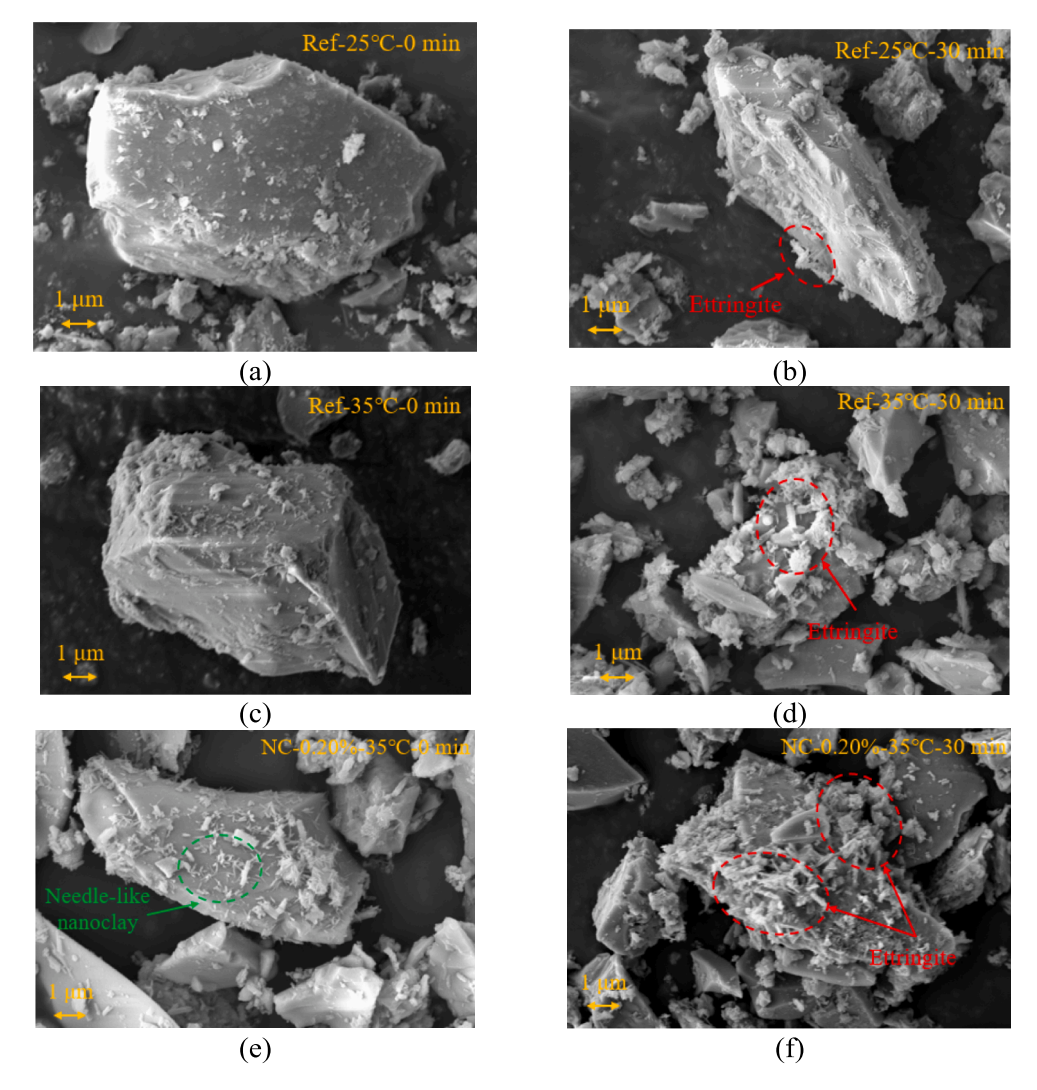


Fig. 14. SEM pictures of investigated UHPC pastes at different stages of hydration: (a) particles surface of Ref at 25 °C hydrated for 0 min; (b) particles surface of Ref at 25 °C hydrated for 30 min; (c) particles surface of Ref at 35 °C hydrated for 0 min; (d) particles surface of Ref at 35 °C hydrated for 30 min; (e) particles surface of NC-0.20% at 35 °C hydrated for 0 min; (f) particles surface of NC-0.20% at 35 °C hydrated for 30 min.

The early chemical hydrations of cement-based materials are primarily controlled by two reactions: (1) the silicate reaction and (2) the aluminate reaction. The silicate and aluminate reaction are represented schematically by Eq. (4) and Eq. (5). Specifically, the silicate reaction leads to the precipitation of C—S—H and portlandite [76]. In addition, the aluminate reaction mainly leads to the formation of ettringite [77].

$$C_3S + Water \rightarrow C - S - H + Portlandite$$
 (4)

$$C_3A + Calcium Sulfate + Water \rightarrow Ettringite$$
 (5)

The representative XRD results for Ref and NC-0.20% at different ambient temperatures (e.g., $10\,^{\circ}$ C, $25\,^{\circ}$ C, and $35\,^{\circ}$ C) were plotted in Fig. A2 in Appendix. Based on that, Fig. 13 plots the quantitative evolution of the phase change of UHPC pastes in the first 30 mins which was determined by the Rietveld refinements method. Besides, the external standard method was applied and weight percentage (i.e., wt, %) are the absolute values of all phases including the significant amorphous content and the not determined phases. Several key phenomena were revealed for UHPC pastes hydration process within the first 30 min: (1) No significant C_3S dissolution as well as no significant C—S—H and portlandite precipitation were found for both Ref and NC-0.20%. (2) Significant C_3A dissolution and significant newly formed ettringite were found for both Ref and NC-0.20%. (3) Both high temperatures and

nanoclay additions increased the ettringite formation. For instance, as the temperature increased from 10 °C to 35 °C, the newly formed ettringite increased from 1.1% to 2.0% for Ref. The underlying mechanism is due to the high temperature increased the dissolution of C_3A , promoting the ettringite formation [78]. In addition, as the nanoclay content increased to 0.20%, the newly formed ettringite increased from 1.5% to 1.7% at 25 °C because nanoclay with high aluminates alters the sulfate-aluminate balance in the solution, resulting in secondary hydration of C_3A to generate more ettringite [74]. Therefore, it could be reasoned, aluminate reaction is the primary hydration reaction in the first 30 min and ettringite is the main hydration product to affect the rheological properties of UHPC pastes. Moreover, compared to the nanoclay addition, the higher ambient temperature shows more pronounced effect on ettringite formation.

4.7. SEM observations

The SEM pictures of cementitious materials particles of UHPC pastes at different hydration stages were shown in Fig. 14. For the reference UHPC paste (i.e., Ref), the surfaces of the unhydrated particles (i.e., hydration time is 0 min) were bare, with debris lying on the top shown in Fig. 14(a) and Fig. 14(c). After 30 min of hydration process, some needle-like structures were found on the surface of cementitious

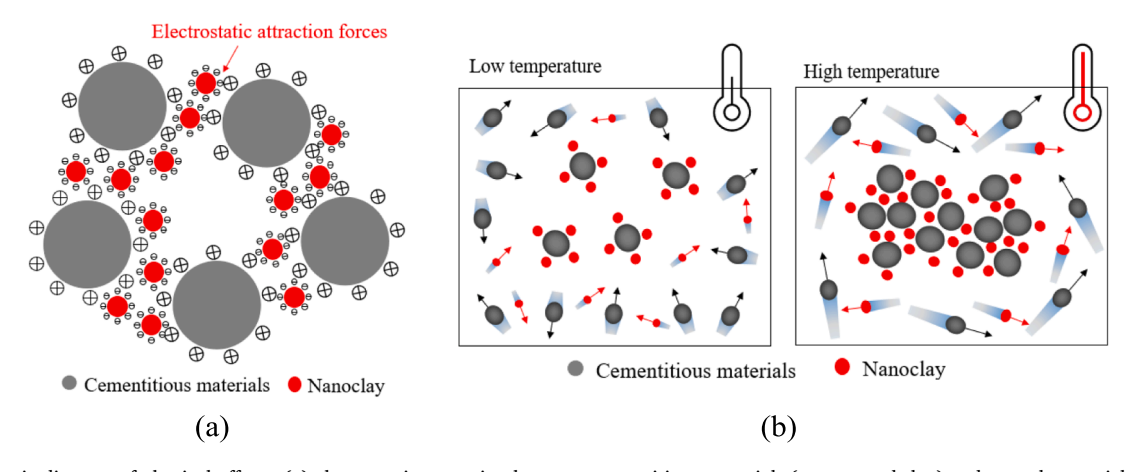


Fig. 15. Schematic diagram of physical effects: (a) electrostatic attraction between cementitious materials (cement and slag) and nanoclay particles; and (b) promoted Brownian motions of particles due to the high ambient temperature.

materials shown in Fig. 14(b) and Fig. 14(d). According to the quantitative XRD results in Section 4.6, the early-age hydration products should be ettringite, which is indeed the needle-like structure [79]. For the UHPC paste with nanoclay addition (i.e., NC-0.20%), the surfaces of the unhydrated particles (i.e., hydration time is 0 min) were bare, with some nanoclay particles lying on the top shown in Fig. 14(e). After 30 min of hydration process, a large amount of ettringite were found on the surface of cementitious materials shown in Fig. 14(f).

In summary, the SEM observation showed that: (1) after 30 min hydration, a small amount of hydration products (i.e., ettringite) were formed on the surface of cementitious materials particles. (2) the high ambient temperature and the addition of nanoclay significantly increased the formation of the ettringite, which is also validated in Section 4.6.

5. Discussions

5.1. Physical effect

The physical effects refer to the flocculation between particles due to the electrostatic forces. First, the mineral components of unhydrated cement particles are tricalcium silicate (C_3S), dicalcium silicate (C_2S), tricalcium aluminate (C_3A), and tetra calcium alumina ferrite (C_4AF). Among them, C_3S and C_2S have negative surface charges, but C_3A and C_4AF have positive surface charges [80]. Thus, nanoclay particles with negative surface charges have a strong affinity to contact with C_3A and C_4AF due to the electrostatic attraction forces shown in Fig. 15(a). The

quick flocculation between particles results in the dramatic initial fluctuation of static yield stress [43]. As reported in Section 4, when nanoclay increased from 0 to 0.20%, the initial fluctuation of static yield stress was increased by 2000% (25 $^{\circ}$ C), which validated the significant flocculation by adding nanoclay.

Besides, the elevation of ambient temperatures also contributes to the flocculation between particles. Higher ambient temperature promotes the Brownian motion of the particles, accelerating the flocculation [81] shown in Fig. 15(b). As reported in Section 4, when ambient temperature increased from 10 °C to 35 °C, the initial fluctuation of static yield stress was increased by 350% (Ref). Compared with the ambient temperature, the nanoclay content shows a higher contribution to the physical effect to increase the rheological properties of UHPC pastes. Moreover, the electrostatic attraction forces between particles can be broken by external interferences, such as agitation and vibration [26]. Thus, the physical flocculation between particles in the early ages is a reversible process. In other words, the development of yield stress and viscosity of fresh UHPC pastes in the early ages can be fully recovered.

5.2. Chemical effect

The chemical effects refer to the enhanced hydration reaction for cementitious materials. On the one hand, the addition of nanoclay increases aluminates contents in the solution, thus promoting the hydration of C_3A to generate more ettringite [74], which were experimentally validated in Section 4.5, 4.6, and 4.7. The newly formed hydration

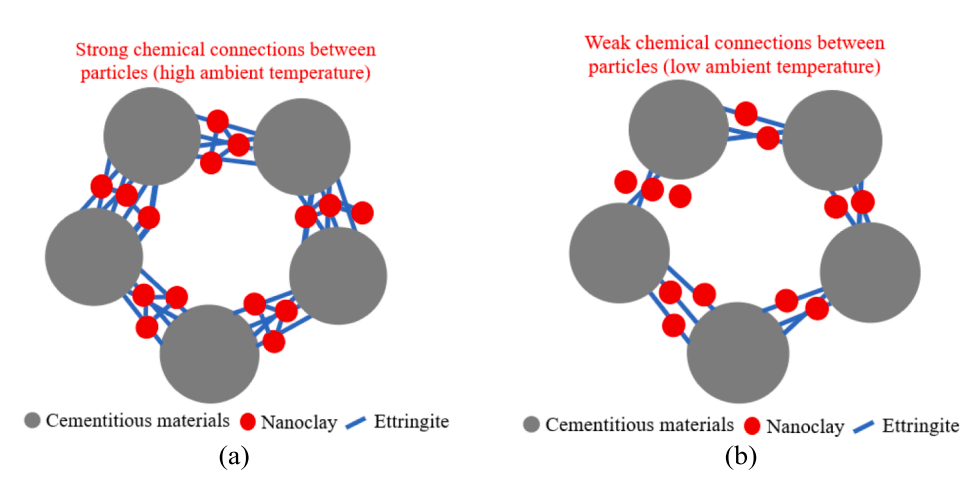


Fig. 16. Schematic diagram of chemical effect: strong hydration reaction connections.

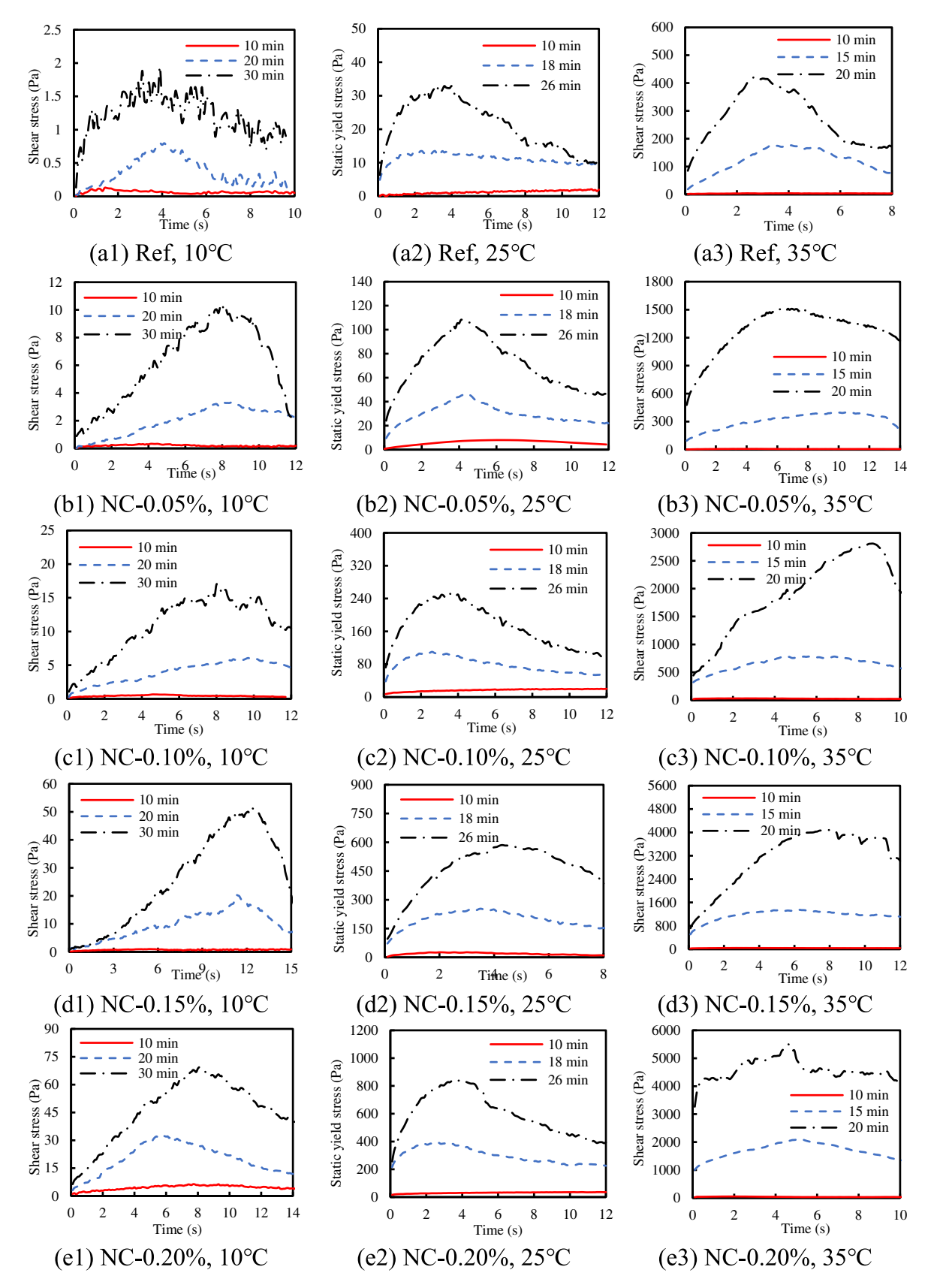


Fig. A1. The representative shear stress-shear time curves for UHPC pastes: (a) Ref; (b) NC-0.05%; (c) NC-0.10%; (c) NC-0.15%; and (d) NC-0.20%.

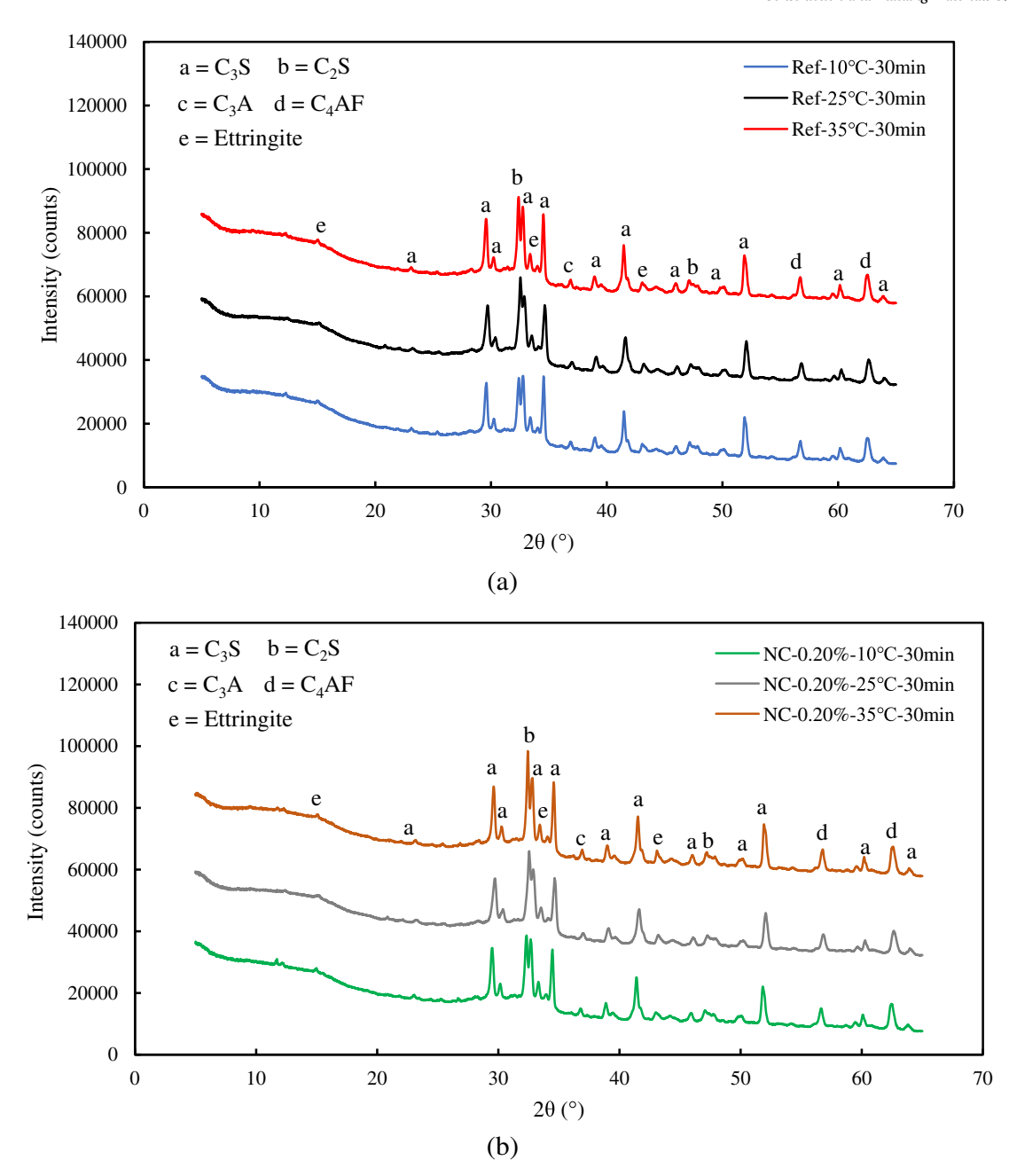


Fig. A2. The representative results of the XRD tests for UHPC pastes (e.g., Ref and NC-0.20%) at 10 °C, 25 °C, and 35 °C.

products (i.e., ettringite) behave with a bridge effect which efficiently connects adjacent particles shown in Fig. 16, resulting in the development of the thixotropy index. For instance, when nanoclay increased from 0 to 0.20%, the thixotropy index was increased by 2400% (25 $^{\circ}$ C).

On the other hand, the elevation of ambient temperatures increases the dissolution of cementitious particles then promotes the chemical hydration reaction [78]. As reported in Section 4, when the ambient temperature increased from 10 $^{\circ}\text{C}$ to 35 $^{\circ}\text{C}$, the thixotropy index was increased by 15000% (Ref). Compared with the nanoclay contents, the ambient temperatures show a higher contribution to the chemical effect to increase the rheological properties of UHPC pastes. Furthermore, different from the electrostatic attraction forces between particles, the enhanced chemical hydration is irreversible progress.

6. Conclusion

The commercial uniformly dispersed and water-based nanoclay

suspension was proved to be an effective rheology modified admixture for UHPC pastes. In addition, the coupled effect and underlying mechanism of water-based nanoclay and ambient temperatures on the rheological properties of UHPC pastes were investigated. According to experimental results, the following conclusions are proposed:

- (1) The total organic carbon test indicated that the adsorption rate of the water-based nanoclay used in this study is calculated as 47.9 mg/g of HRWR, which is acceptable and compatible with common-used PCE-based HRWR for UHPC pastes.
- (2) The coupled effect of nanoclay contents and ambient temperatures efficiently reduced the workability of UHPC pastes due to the accelerated flocculation and water absorption capacity of nanoclay. As the nanoclay content increased from 0 to 0.20%, the mini-slump spreads were reduced by 29%, 45%, and 47% at $10~^{\circ}$ C, $25~^{\circ}$ C, and $35~^{\circ}$ C.

- (3) The coupled effect of nanoclay contents and ambient temperatures efficiently enhanced the dynamic yield stress and plastic viscosity of UHPC pastes. As the nanoclay content increased from 0 to 0.20%, the dynamic yield stresses were increased by 180%, 270%, and 490% and the plastic viscosity were increased by 80%, 110%, and 65% at 10 °C, 25 °C, and 35 °C. The coupled effect is much more pronounced on the development of the dynamic yield stress.
- (4) The coupled effect of nanoclay and ambient temperature significantly enhanced the thixotropy of UHPC pastes, including initial fluctuations of static yield stress ($\tau_{\rm floc}$) and thixotropy index (I_A). As the nanoclay content increased from 0 to 0.20%, the $\tau_{\rm floc}$ was ranged from 0.7 Pa to 2.8 Pa, from 1.2 Pa to 27.7 Pa, and from 3.1 Pa to 38.7 Pa, at 10 °C, 25 °C, and 35 °C, respectively. The evolution of $\tau_{\rm floc}$ was mainly related to the physical effect: accelerated flocculation between particles by electrostatic attraction forces.
- (5) As the nanoclay content increased from 0 to 0.20%, the I_A was ranged from 0.1 Pa/min to 3.2 Pa/min, from 2.0 Pa/min to 50.6 Pa/min, and from 42.0 Pa/min to 545.2 Pa/min at 10 °C, 25 °C, and 35 °C, respectively. The evolution of I_A was due to the sum of the physical effect (i.e., accelerated flocculation) and chemical hydration reactions (i.e., the formation of ettringite).
- (6) The results of isothermal calorimetry analysis, quantitative XRD analysis, and SEM observation revealed that the coupled effect of nanoclay contents and ambient temperature significantly promoted the initial hydration (i.e., within 1 h), which leads to the quick growth of thixotropy index I_A. Compared to nanoclay contents, the ambient temperature plays the dominant impact in this stage. Moreover, ettringite is the main hydration product to affect the rheological properties of UHPC pastes

CRediT authorship contribution statement

Jiang Du: Data curation, Formal analysis, Investigation, Visualization, Writing – original draft. **Pengwei Guo:** Data curation, Validation, Writing – review & editing. **Weina Meng:** Conceptualization, Project administration, Resources, Supervision, Funding acquisition, Writing – review & editing.

Declaration of Competing Interest

The authors declare that they have no known competing financial interests or personal relationships that could have appeared to influence the work reported in this paper.

Data availability

Data will be made available on request.

Acknowledgments

This research is supported by the National Science Foundation [grant number CMMI-2046407] and New Jersey Department of Transportation: Task Order 388 – Bridge Resource Program (2021-2022), contract ID number: 21-50862. The authors also would like to thank ActiveMinerals International Company (https://activeminerals.com) for the donation of water-based nanoclay (Model: Liquid Acti-Gel 208).

Appendix

References

- [1] J. Du, W. Meng, K.H. Khayat, Y. Bao, P. Guo, Z. Lyu, A. Abu-obeidah, H. Nassif, H. Wang, New development of ultra-high-performance concrete (UHPC), Composites Part B: Eng. (2021) 109220.
- [2] W. Meng, K.H. Khayat, Improving flexural performance of ultra-high-performance concrete by rheology control of suspending mortar, Compos. B Eng. 117 (2017) 26–34.
- [3] J. Du, Z. Liu, C. Christodoulatos, M. Conway, Y. Bao, W. Meng, Utilization of off-specification fly ash in preparing ultra-high-performance concrete (UHPC): Mixture design, characterization, and life-cycle assessment, Resour. Conserv. Recycl. 180 (2022), 106136.
- [4] T. Alahmari, C. Kennedy, A. Cuaron, B. Weldon, D. Jauregui, Field testing of a prestressed concrete bridge with high performance and locally developed ultrahigh performance girders, Front. Built Environ. 5 (2019) 114.
- [5] S. Aaleti, S. Sritharan, A. Abu-Hawash, Innovative UHPC-normal concrete composite bridge deck. Proceedings of the RILEM-fib-AFGC International Symposium on Ultra-High Performance Reinforced Concrete, Eds: F. Toutlemonde, J. Resplendino, Rilem Publications SARL, Bagneux, France, 2013.
- [6] T.V. Voort, M.T. Suleiman, S. Sritharan, Design and performance verification of ultra-high performance concrete piles for deep foundations, Iowa State University. Center for Transportation Research and Education, 2008.
- [7] J. Qi, Y. Bao, J. Wang, L. Li, W. Li, Flexural behavior of an innovative dovetail UHPC joint in composite bridges under negative bending moment, Eng. Struct. 200 (2019) 109716
- [8] Graybeal, B., Field-cast UHPC connections for modular bridge deck elements. 2010..
- [9] B.A. Graybeal, Ultra-High Performance Concrete Composite Connections For Precast Concrete Bridge Decks. 2012, United States, Federal Highway Administration. Office of Infrastructure Research and Development, 2012.
- [10] S. Verger-Leboeuf, J.-P. Charron, B. Massicotte, Design and behavior of UHPFRC field-cast transverse connections between precast bridge deck elements, J. Bridg. Eng. 22 (7) (2017) 04017031.
- [11] J. Xie, Q. Fu, J.-B. Yan, Compressive behaviour of stub concrete column strengthened with ultra-high performance concrete jacket, Constr. Build. Mater. 204 (2019) 643–658.
- [12] Z.B. Haber, J.F. Munoz, B.A. Graybeal, Field Testing Of An Ultra-High Performance Concrete Overlay, Federal Highway Administration. Office of Infrastructure Research & Development Federal Highway Administration, 2017.
- [13] K.H. Khayat, M. Valipour, Design of ultra high performance concrete as an overlay in pavements and bridge decks, Missouri University of Science and Technology. Center for Transportation Infrastructure and Safety, 2014.
- [14] Z.B. Haber, J.F. Munoz, I. De la Varga, B.A. Graybeal, Bond characterization of UHPC overlays for concrete bridge decks: Laboratory and field testing, Constr. Build. Mater. 190 (2018) 1056–1068.
- [15] H. Wibowo, S. Sritharan, Use of Ultra-High-Performance Concrete For Bridge Deck Overlays, Federal Highway Administration, United States, 2018.
- [16] P. Mazzacane, R. Ricciotti, F. Teply, E. Tollini, D. Corvez, MUCEM: The builder's perspective, Proc. UHPFRC (2013) 3–16.
- [17] S. Aubry, P. Bompas, B. Vaudeville, D. Corvez, T. Lagrange, P. Mazzacane, A. Brizou, A UHPFRC cladding challenge: the fondation Louis Vuitton pour la création" Iceberg". 2nd RILEM-fib-AFGC International Symposium on Ultra-High Performance Fibre-Reinforced Concrete, 2013.
- [18] N. Gaudillière, R. Duballet, C. Bouyssou, A. Mallet, P. Roux, M. Zakeri, J. Dirrenberger, Large-scale additive manufacturing of ultra-high-performance concrete of integrated formwork for truss-shaped pillars. Robotic Fabrication in Architecture, Art and Design, Springer, 2018.
- [19] K.H. Khayat, W. Meng, K. Vallurupalli, L. Teng, Rheological properties of ultrahigh-performance concrete—An overview, Cem. Concr. Res. 124 (2019), 105828.
- [20] A.F. Omran, K.H. Khayat, Choice of thixotropic index to evaluate formwork pressure characteristics of self-consolidating concrete, Cem. Concr. Res. 63 (2014) 89–97.
- [21] Y. Xie, D.J. Corr, M. Chaouche, F. Jin, S.P. Shah, Experimental study of filling capacity of self-compacting concrete and its influence on the properties of rockfilled concrete, Cem. Concr. Res. 56 (2014) 121–128.
- [22] G. De Schutter, K. Lesage, V. Mechtcherine, V.N. Nerella, G. Habert, I. Agusti-Juan, Vision of 3D printing with concrete — Technical, economic and environmental potentials, Cem. Concr. Res. 112 (2018) 25–36.
- [23] A. Kostrzanowska-Siedlarz, J. Gołaszewski, Rheological properties of high performance self-compacting concrete: effects of composition and time, Constr. Build. Mater. 115 (2016) 705–715.
- [24] C.F. Ferraris, J.M. Gaidis, Connection between the rheology of concrete and rheology of cement paste, Mater. J. 89 (4) (1992) 388–393.
- [25] A. Peyvandi, L.A. Sbia, P. Soroushian, K. Sobolev, Effect of the cementitious paste density on the performance efficiency of carbon nanofiber in concrete nanocomposite, Constr. Build. Mater. 48 (2013) 265–269.
- [26] J. Assaad, K.H. Khayat, H. Mesbah, Assessment of thixotropy of flowable and self-consolidating concrete, Mater. J. 100 (2) (2003) 99–107.
- [27] R. Saleh Ahari, T. Kemal Erdem, K. Ramyar, Effect of various supplementary cementitious materials on rheological properties of self-consolidating concrete, Constr. Build. Mater. 75 (2015) 89–98.
- [28] C. Jayasree, R. Gettu, Experimental study of the flow behaviour of superplasticized cement paste, Mater. Struct. 41 (9) (2008) 1581–1593.
- [29] J. Du, P. Guo, Z. Liu, W. Meng, Highly thixotropic ultra-high-performance concrete (UHPC) as an overlay, Constr. Build. Mater. 366 (2023), 130130.

- [30] R. Wang, X. Gao, H. Huang, G. Han, Influence of rheological properties of cement mortar on steel fiber distribution in UHPC, Constr. Build. Mater. 144 (2017) 65–73.
- [31] A. Mardani-Aghabaglou, M. Tuyan, G. Yılmaz, Ö. Ariöz, K. Ramyar, Effect of different types of superplasticizer on fresh, rheological and strength properties of self-consolidating concrete, Constr. Build. Mater. 47 (2013) 1020–1025.
- [32] H. Feng, Z. Feng, W. Wang, Z. Deng, B. Zheng, Impact of polycarboxylate superplasticizers (PCEs) with novel molecular structures on fluidity, rheological behavior and adsorption properties of cement mortar, Constr. Build. Mater. 292 (2021), 123285.
- [33] R. Jing, Y. Liu, P. Yan, Uncovering the effect of fly ash cenospheres on the macroscopic properties and microstructure of ultra high-performance concrete (UHPC), Constr. Build. Mater. 286 (2021), 122977.
- [34] G. Ling, Z. Shui, T. Sun, X. Gao, Y. Wang, Y. Sun, G. Wang, Z. Li, Rheological behavior and microstructure characteristics of SCC incorporating metakaolin and silica fume, Materials 11 (12) (2018) 2576.
- [35] R. Yu, F. Zhou, T. Yin, Z. Wang, M. Ding, Z. Liu, Y. Leng, X. Gao, Z. Shui, Uncovering the approach to develop ultra-high performance concrete (UHPC) with dense meso-structure based on rheological point of view: Experiments and modeling, Constr. Build. Mater. 271 (2021), 121500.
- [36] S. Ma, Y. Qian, S. Kawashima, Experimental and modeling study on the non-linear structural build-up of fresh cement pastes incorporating viscosity modifying admixtures, Cem. Concr. Res. 108 (2018) 1–9.
- [37] L. Teng, W. Meng, K.H. Khayat, Rheology control of ultra-high-performance concrete made with different fiber contents, Cem. Concr. Res. 138 (2020), 106222.
- [38] L. Teng, H. Huang, J. Du, K. Khayat, Prediction of fiber orientation and flexural performance of UHPC based on suspending mortar rheology and casting method, Cem. Concr. Compos. (2021).
- [39] L. Teng, J. Zhu, K.H. Khayat, J. Liu, Effect of welan gum and nanoclay on thixotropy of UHPC, Cem. Concr. Res. 138 (2020), 106238.
- [40] S. Kawashima, K. Wang, R.D. Ferron, J.H. Kim, N. Tregger, S. Shah, A review of the effect of nanoclays on the fresh and hardened properties of cement-based materials, Cem. Concr. Res. 147 (2021), 106502.
- [41] D. Jiao, R. De Schryver, C. Shi, G. De Schutter, Thixotropic structural build-up of cement-based materials: A state-of-the-art review, Cem. Concr. Compos. (2021), 104152.
- [42] P. Guo, J. Du, Y. Bao, W. Meng, Real-time video recognition for assessing plastic viscosity of ultra-high-performance concrete (UHPC), Measurement 191 (2022), 110809.
- [43] Qian, Y., Characterization of structural rebuilding and shear migration in cementitious materials in consideration of thixotropy (Doctoral dissertation).
- [44] Y. Qian, G. De Schutter, Enhancing thixotropy of fresh cement pastes with nanoclay in presence of polycarboxylate ether superplasticizer (PCE), Cem. Concr. Res. 111 (2018) 15–22.
- [45] L. Lei, J. Plank, A concept for a polycarboxylate superplasticizer possessing enhanced clay tolerance, Cem. Concr. Res. 42 (10) (2012) 1299–1306.
- [46] Y. Qian, S. Kawashima, Use of creep recovery protocol to measure static yield stress and structural rebuilding of fresh cement pastes, Cem. Concr. Res. 90 (2016) 73,79
- [47] S. Kawashima, J.H. Kim, D.J. Corr, S.P. Shah, Study of the mechanisms underlying the fresh-state response of cementitious materials modified with nanoclays, Constr. Build. Mater. 36 (2012) 749–757.
- [48] H. Varela, G. Barluenga, I. Palomar, Influence of nanoclays on flowability and rheology of SCC pastes, Constr. Build. Mater. 243 (2020), 118285.
- [49] H. Huang, T. Huang, Q. Yuan, D. Zhou, D. Deng, L. Zhang, Temperature dependence of structural build-up and its relation with hydration kinetics of cement paste, Constr. Build. Mater. 201 (2019) 553–562.
- [50] A.R. Jayapalan, M.L. Jue, K.E. Kurtis, Nanoparticles and apparent activation energy of Portland cement, J. Am. Ceram. Soc. 97 (5) (2014) 1534–1542.
- [51] Y. Sargam, K. Wang, Hydration kinetics and activation energy of cement pastes containing various nanoparticles, Compos. B Eng. 216 (2021), 108836.
- [52] M. Nehdi, S. Al Martini, Estimating time and temperature dependent yield stress of cement paste using oscillatory rheology and genetic algorithms, Cem. Concr. Res. 39 (11) (2009) 1007–1016.
- [53] W. Meng, K.H. Khayat, Effect of graphite nanoplatelets and carbon nanofibers on rheology, hydration, shrinkage, mechanical properties, and microstructure of UHPC, Cem. Concr. Res. 105 (2018) 64–71.
- [54] Z. Liu, J. Du, W. Meng, Achieving low-carbon cementitious materials with high mechanical properties using CaCO3 suspension produced by CO2 sequestration, J. Clean. Prod. 373 (2022), 133546.

- [55] M.S. Konsta-Gdoutos, Z.S. Metaxa, S.P. Shah, Highly dispersed carbon nanotube reinforced cement based materials, Cem. Concr. Res. 40 (7) (2010) 1052–1059.
- [56] A. Peyvandi, P. Soroushian, N. Abdol, A.M. Balachandra, Surface-modified graphite nanomaterials for improved reinforcement efficiency in cementitious paste, Carbon 63 (2013) 175–186.
- [57] Kausar, A., 7 Flame retardant potential of clay nanoparticles, in Clay Nanoparticles, G. Cavallaro, R. Fakhrullin, and P. Pasbakhsh, Editors. 2020, Elsevier. p. 169-184.
- [58] Y. Qian, K. Lesage, K. El Cheikh, G. De Schutter, Effect of polycarboxylate ether superplasticizer (PCE) on dynamic yield stress, thixotropy and flocculation state of fresh cement pastes in consideration of the Critical Micelle Concentration (CMC), Cem. Concr. Res. 107 (2018) 75–84.
- [59] Standard Specification for Flow Table for Use in Tests of Hydraulic Cement. 2014, ASTM International.
- [60] C. Hu, F. de Larrard, The rheology of fresh high-performance concrete, Cem. Concr. Res. 26 (2) (1996) 283–294.
- [61] M. Ding, R. Yu, Y. Feng, S. Wang, F. Zhou, Z. Shui, X. Gao, Y. He, L. Chen, Possibility and advantages of producing an ultra-high performance concrete (UHPC) with ultra-low cement content, Constr. Build. Mater. 273 (2021), 122023.
- [62] Q. Yuan, D. Zhou, K.H. Khayat, D. Feys, C. Shi, On the measurement of evolution of structural build-up of cement paste with time by static yield stress test vs. small amplitude oscillatory shear test, Cem. Concr. Res. 99 (2017) 183–189.
- [63] A.M. Mostafa, A. Yahia, New approach to assess build-up of cement-based suspensions, Cem. Concr. Res. 85 (2016) 174–182.
- [64] N. Roussel, Steady and transient flow behaviour of fresh cement pastes, Cem. Concr. Res. 35 (9) (2005) 1656–1664.
- [65] J. Kruger, S. Zeranka, G. van Zijl, 3D concrete printing: a lower bound analytical model for buildability performance quantification, Autom. Constr. 106 (2019), 102004
- [66] S. Ma, S. Kawashima, A rheological approach to study the early-age hydration of oil well cement: Effect of temperature, pressure and nanoclay, Constr. Build. Mater. 215 (2019) 119–127.
- [67] Scrivener, K., Snellings, R., and Lothenbach, B., A practical guide to microstructural analysis of cementitious materials. 2018: CRC Press.
- [68] S. Sui, W. Wilson, F. Georget, H. Maraghechi, H. Kazemi-Kamyab, W. Sun, K. Scrivener, Quantification methods for chloride binding in Portland cement and limestone systems, Cem. Concr. Res. 125 (2019), 105864.
- [69] R.J. Flatt, Y.F. Houst, A simplified view on chemical effects perturbing the action of superplasticizers. Cem. Concr. Res. 31 (8) (2001) 1169–1176.
- [70] S. Ng, J. Plank, Interaction mechanisms between Na montmorillonite clay and MPEG-based polycarboxylate superplasticizers, Cem. Concr. Res. 42 (6) (2012) 847–854
- [71] G.H. Tattersall, Workability and quality control of concrete, CRC Press, 1991.
- [72] I. Dejaeghere, M. Sonebi, G. De Schutter, Influence of nano-clay on rheology, fresh properties, heat of hydration and strength of cement-based mortars, Constr. Build. Mater. 222 (2019) 73–85.
- [73] M. Şahmaran, Z. Bilici, E. Ozbay, T.K. Erdem, H.E. Yucel, M. Lachemi, Improving the workability and rheological properties of Engineered Cementitious Composites using factorial experimental design, Compos. B Eng. 45 (1) (2013) 356–368.
- [74] A. Quennoz, K.L. Scrivener, Interactions between alite and C3A-gypsum hydrations in model cements, Cem. Concr. Res. 44 (2013) 46–54.
- [75] Griesser, A., Cement-superplasticizer interactions at ambient temperatures (Doctoral dissertation). 2002.
- [76] C. Jakob, D. Jansen, N. Ukrainczyk, E. Koenders, U. Pott, D. Stephan, J. Neubauer, Relating ettringite formation and rheological changes during the initial cement hydration: a comparative study applying XRD analysis, rheological measurements and modeling, Materials 12 (18) (2019) 2957.
- [77] H.F. Taylor, Cement Chemistry, Vol. 2, Thomas Telford London, 1997.
- [78] J. Bensted, Effects of the clinker-gypsum grinding temperature upon early hydration of Portland cement, Cem. Concr. Res. 12 (3) (1982) 341–348.
- [79] R. Ylmén, U. Jäglid, B.-M. Steenari, I. Panas, Early hydration and setting of Portland cement monitored by IR, SEM and Vicat techniques, Cem. Concr. Res. 39 (5) (2009) 433–439.
- [80] K. Yoshioka, E.-I. Tazawa, K. Kawai, T. Enohata, Adsorption characteristics of superplasticizers on cement component minerals, Cem. Concr. Res. 32 (10) (2002) 1507–1513.
- [81] N. Roussel, G. Ovarlez, S. Garrault, C. Brumaud, The origins of thixotropy of fresh cement pastes, Cem. Concr. Res. 42 (1) (2012) 148–157.